University of Nevada, Reno

Verification and Development of a Steady Thermal CFD Model for High Density Staging of Radiological Materials Packages

A thesis submitted in partial fulfillment of the
requirements for the degree of Master of Science in
Mechanical Engineering

By:

Matthew Murphy-Sweet

Dr. Miles Greiner, PhD

Dr. Mustafa Hadj-Nacer, PhD

May, 2024

This work was done by Mission Support and Test Services, LLC, under Contract No. DENA0003624 with the U.S. Department of Energy Office of Environment, Health, Safety and Security, and the Office of Nuclear Safety. DOENV/03624--1965.

THE GRADUATE SCHOOL

We recommend that the thesis
prepared under our supervision by

Matthew Murphy-Sweet

entitled

Verification and Development of a Steady Thermal CFD Model for High Density Staging of Radiological Materials Packages

be accepted in partial fulfillment of the
requirements for the degree of

MASTER OF SCIENCE

Miles Greiner, Ph.D.
Advisor

Mustafa Hadj-Nacer, Ph.D.
Co-advisor

Nicholas Tsoulfanidis, Ph.D.
Graduate School Representative

Markus Kemmelmeier, Ph.D., Dean
Graduate School

May, 2024

Abstract

This thesis overviews the work that took place to exercise and verify results of a computational fluid dynamics model with a densely-packed array of staged heat generating packages in a theoretical ventilated room for the purposes of developing an application that estimates the surface temperatures of the packages with configurable loading conditions. A generic staging building was modelled in Solidworks with lights, a ventilation system, and 640 packages containing radiological materials placed on pallets located on four racks. The geometry was then used in Ansys Workbench where fluid and solid regions were assigned and then meshed with four different grid sizes.

In Ansys Fluent, these regions were assigned boundary conditions and material properties that replicate a realistic loading condition for the theoretical staging room. Package temperature results from each mesh were compared with one another to determine the number of iterations and grid size necessary to approach the results achieved by the finest grid for 10,000 iterations. The results of the finest grid sizing are used to present the expected flow pattern in the staging building, the distribution of package temperatures, and the location of the packages of interest.

From this work, the grid sizing and number of iterations needed for the simulation for the application were found to be 64 million elements run for 7,000 iterations. Package temperatures from the finest grid result indicate that the maximum package surface temperatures do not exceed 43^{o}C which is 6.4^{o}C colder than the maximum allowable surface temperature of the 9975 package.

Acknowledgements

First and foremost, I would love to thank my advisors, Miles Greiner and Mustafa Hadj-Nacer for the opportunity to learn and develop the skills of thermal analysis in the realm of computational fluid dynamics. Thanks to Frank Pulciano for his collaboration and daily encouragement. Their contributions and encouragement in my education has started me on a path in the nuclear industry that I expect to continue down the rest of my life. Additionally, I would like to thank Dr. Tsoulfanidis for his teaching and his participation in my thesis committee.

It goes without saying that I wouldn't be in the position I'm in today without the love and support of my family. My parents, grandparents, and siblings have been the driving force behind my success all my life. I would like to give a special thanks to my father, Michael Murphy-Sweet, who has always been an example of hard work and first sparked my interest in fluid flows and heat transfer and my high school engineering teacher, Dennis Zattiero, who taught me the tools to succeed in engineering.

Lastly, I would love to thank my wife and daughter, Genevra and Rebekah Murphy-Sweet, and all my friends, who walked alongside me as I completed my master's degree. You all made Reno my home the last two years and I can't wait to see what we do next.

Table of Contents

List of Tables

Tables

List of Figures

Figures

Nomenclature

Abbreviations

CFD	Computational Fluid Dynamics
CFR	Code of Federal Regulation

Units

°C	Degrees Celsius
cfm	Cubic feet per minute
hr	Hours
°F	Degrees Fahrenheit
ft	Feet
kg	Kilogram
K	Kelvin
m	Meters
Pa	Pascal
s	Second
W	Watt
J	Joule

Letters

A	Area
c_p	Specific Heat
i	Number of Iterations (1, 2, … 10,000)
k	Thermal Conductivity
$\dot{m}$	Mass Flow Rate
N	Number of Elements
$\dot{Q}$	Heat Generated
P	Pressure
S	Standard Error of Estimate
T	Temperature
t	Time
μ	Kinematic Viscosity

Symbols

ε	Emissivity
ρ	Density
2σ	Two Standard Deviations

Subscripts

95	95% Confidence Level
avg	Average Over Surface
comp	Computational
exc	Excluding the Top Packages in Racks 1 and 4
EB	Energy Balance
F	Fluid

in	Air Inlet
L	Light
max	Maximum Over Surface
pg	Package
PGmax	Mean of the Package Maximum Temperatures
out	Air Outlet
S	Solid
tot	Total

1 Introduction

1.1 Background

The Model 9975 Package is designed for transportation and storage of radiological material [1]. It consists of a stainless-steel primary containment vessel nested within a secondary stainless steel containment vessel. These vessels are supported by shock and absorbing plates within a 0.53-m (1.76-ft) diameter, 0.91-m (3.00-ft) outer stainless-steel shell. Celotex insulation fills the regions between the containment vessels and outer shell. Radiological materials that generate up to $\dot{Q}_{pg}$ = 19 W of thermal energy are placed within the primary containment vessel. Under some conditions, packages may be staged together in dense configurations. The heat output from multiple packages can be managed by air-conditioning systems in temperature-controlled rooms.

The Code of Federal Regulations (10 CFR 71) describes conditions that all radiological material transport and storage packages must meet [2]. These packages must contain the material, shield the surrounding from harmful radiation, and provide criticality-safety under normal conditions of transport (NCT) and hypothetical accident conditions (HAC). NCT are characterized by an environment temperature of 38°C (100°F), and specified insolation. To facilitate package handling, no exposed surface may exceed 50°C (122°F).

1.2 Hypothetical Staging Room

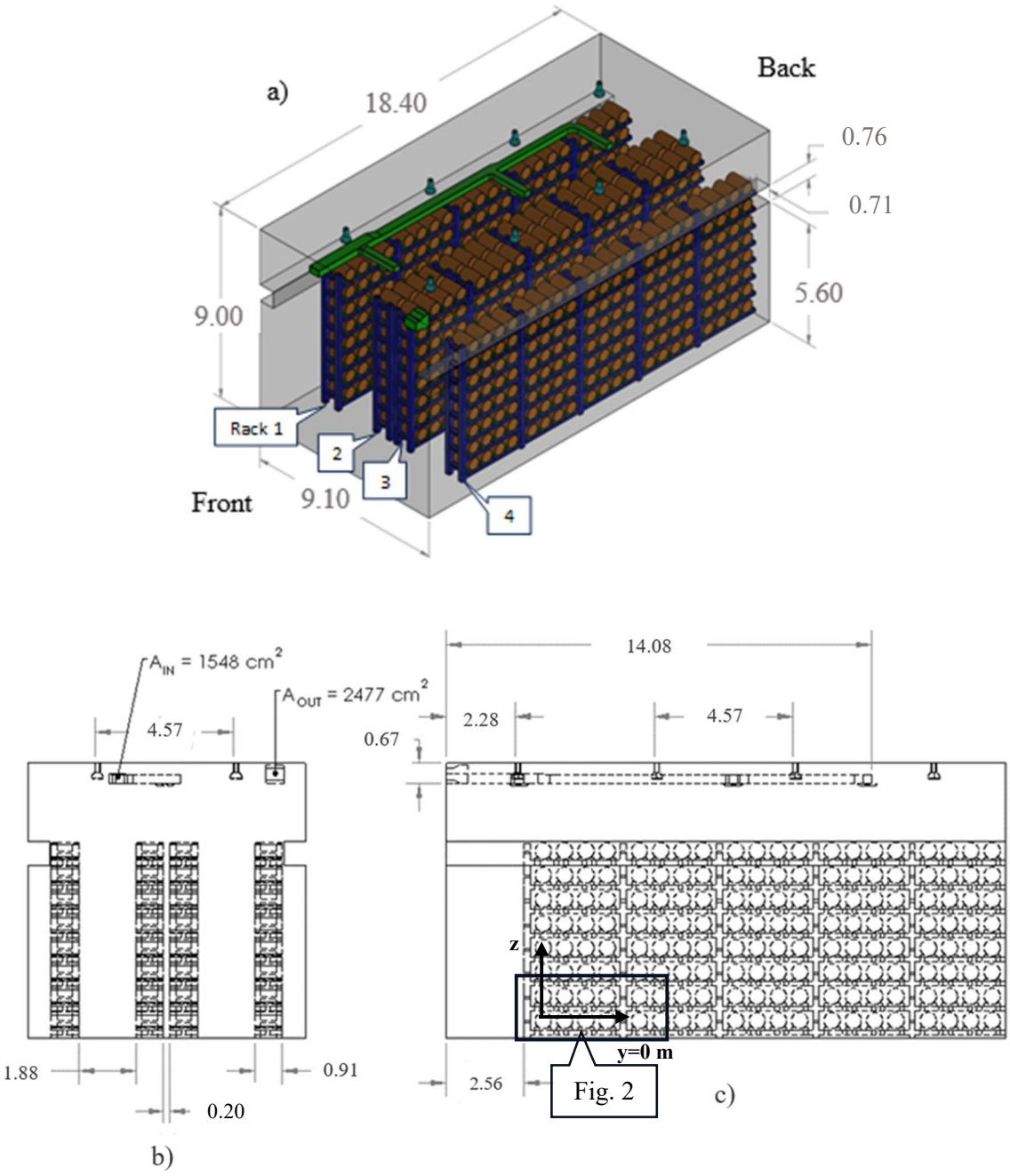

Figure 1: Components of the hypothetical staging room from a) three-dimensional, b) cross sectional, and c) axial view. All dimensions are in meters unless noted.

Figure 1 shows the components and dimensions of a hypothetical staging room being evaluated in this paper. The room is 9.1 m (30 ft) wide, 18.40 m (60.50 ft) long, and 9.00 m (29.50 ft) tall. A 14.08 m (46.06 ft) long air-conditioning supply duct spans

almost the entire room length. Cool air enters the duct inlet that has a cross-sectional area of 1548 cm^2 at the front of the room with a steady mass flow rate of $\dot{m}_{in}$ = 0.784 kg/s (1370 cfm) and temperature of T_{in} = 17.78°C (64°F). The duct has three legs, with each successive leg being thinner than the last, to evenly distribute the air mass flow rate. The air leaving each leg is directed upward by the diffusers. After circulating within the room, the air exits though a short 0.61 m (2.00 ft) long duct with a cross sectional area of 2477 cm^2 and returns to the air conditioning system. All ducts are made of gauge 13 steel. Eight lights with a steel stem are arranged along the ceiling in two rows. Each light generates $\dot{Q}_L$ = 100 W of thermal energy. The facility's outer walls are conservatively assumed to be adiabatic.

In this staging room, 640 model 9975 packages are supported on four racks. The racks are made of square cross section gauge 20 steel tubing which are 0.1 m (0.33 ft) on each side. Each rack is 5.60 m (18.50 ft) tall, 15.84 m (52.00 ft) long, and 0.91 m (3.00 ft) deep. There is a 2.56-m long open space between the wall at the front of the room and the racks. The outer two racks (numbered 1 and 4) are 0.71 m (2.33 ft) from the outer walls. This accommodates two protrusions near the top of the side walls. There are two, 1.88m (6.17 ft) wide aisles, between the two outer and two inner racks (number 2 and 3). Racks 2 and 3 are spaced 0.20 m (0.67 ft) apart. Each of the racks has five bays with eight levels each.

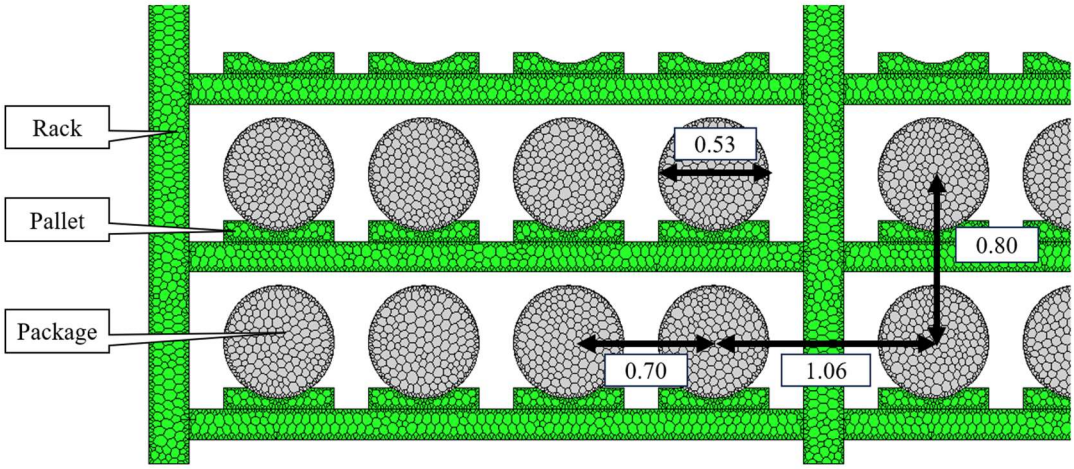

Figure 2: Dimensioned view of the solid components and the spacing of packages in Mesh A

The rectangle in Fig. 1c shows a region encompassing two lower levels of two bays close to the front of the room. An expanded view of that region is shown in Fig. 2. Each level of each bay has four horizontal 9975 packages with center to center spacing of 0.70 m (2.31 ft), on individual latticed, wood pallets. The spacing between packages is 1.06 m (3.50 ft) between bays, and 0.80 m (2.59 ft) between levels.

1.3 Previous Work

Two earlier computational investigations studied the staging room configuration shown in Figs 1 and 2. They considered variations in their representation of the packages and racks. Flynt [3] used Star-CCM+, a commercially available CFD software, with the built-in k-ω turbulence model on a 14.6 million element mesh to evaluate the steady-state thermal response of the room [4]. For simplicity, the four cylindrical packages on each level in each bay were modeled as a single heat generating rectangular box. After evaluating the maximum surface temperature of the boxes for the rooms with eight, nine or ten levels, the study concluded that the room could safely stage eight levels of

packages with the given HVAC system because the simulations with nine and ten shelves resulted in box temperatures above the 50°C maximum.

Kaderka [5] modeled the room in Ansys Fluent [6] using two simplified geometries. The first was rectangular heat generating boxes on racks like the previous work by Flynt. The other was "floating" cylindrical packages in the room without the racks. The goal of that work was to develop a predictive and configurable CFD model. Its objectives were to compare steady-state results from transient simulations to steady simulations and to evaluate the effects of the radiation model. Kaderka determined that temperature results were within 0.1°C between steady and transient simulations but were reached with the shorter computational time using the steady time model. When radiation models were used, the maximum package temperature was one to two degrees lower but required more computational time in the boxes and racks model. Kaderka was not able to identify experimental data that could be used to appropriately validate the simulation results. The most complete model reported a maximum surface temperature of 39.7°C for the hottest package in the floating model.

The motivation for the current study is to continue the work of developing a predictive and configurable CFD-based application to predict maximum package temperatures based upon a user-defined loading scheme of package placements and heat generation rates. Further, the efforts in this work serve to determine the minimal grid refinement needed to produce temperature results for loading configurations and to evaluate the physics phenomena in the defined staging room configuration. In this work, four refined meshes were defined and used in steady-state simulations for 10,000 iterations. The maximum allowed heat generation (19 W) was applied to all 640

packages, and each of the eight lights generated 100 watts, resulting in a total heat generation rate of $\dot{Q}_{tot} = 12{,}960$ watts. The outlet air, package surface average and maximum temperatures, outlet mass flow rate, and pressure difference between the air inlet and out were compared and evaluated between grids to assess the grid and model sensitivity. The discussion and evaluation of results identify the bounding package temperature, define the flow and temperature characteristics of the model, and inform future work for data validation.

2 Computational Methods

2.1 Mesh Generation

The three-dimensional staging room geometry shown in Figs. 1 and 2 was constructed in the commercial CAD modeler Solidworks [7] and then imported into Ansys Workbench as a .stp file. The model was meshed using varying base sizes for the solid and fluid regions using the tetrahedral mesher built-in to Ansys Workbench. Four grids, indexed as k = A, B, C, and D were generated from the refinement of the base size. The base sizes used by region can be found in table 1 with all sizing listed in meters.

Table 1: Base size settings in meters for fluid and solid regions for each mesh

Mesh, k	A	B	C	D
Room Fluid	0.082	0.0651	0.05213	0.04417
Lights	0.0205	0.01627	0.01333	0.01129
Packages	0.0381	0.03024	0.024765	0.02098
Racks	0.041	0.03254	0.02665	0.02258
HVAC Fluid	0.041	0.03254	0.02665	0.02258
Diffuser Fluid	0.02	0.01587	0.013	0.01102
Pallets	0.0381	0.03024	0.024765	0.02098

Table 2: Metrics for the four meshes examined in this work.

Mesh, k	A	B	C	D
$N_{tot,k}$	22,710,929	38,577,680	65,546,591	94,634,880
$N_{F,k}$	18,746,151	30,075,738	50,918,430	71,599,252
$N_{S,k}$	3,964,778	8,501,942	14,628,161	23,035,628
$N_{F,k}/N_{tot,k}$	82.4%	77.9%	77.7%	75.7%
Minimum Grid Orthogonal Quality	0.11	0.10	0.12	0.12
Maximum Grid Aspect Ratio	25	23	19	17
$t_{comp,k}$ [hr]	46.4	75.6	112.8	143.2

For each mesh, Table 2 shows the total number of elements ($N_{tot,k}$), the number of elements in the fluid ($N_{F,k}$) and solid ($N_{S,k}$) regions, and the ratio of fluid elements to the

total. As the grid was refined from the coarsest mesh (A) to the finest mesh (D), the fraction of fluid elements to total elements decreased from 82.4% to 75.7%.

Orthogonal grid quality is a measure of cell edge perpendicularity. If a cell is a perfect cube, the orthogonal quality is one, while a cell with self-intersecting edges has an orthogonal quality of zero. The minimum orthogonal quality is a measure of the lowest quality cell in the mesh. The Ansys Fluent Guide [5] states that the minimum orthogonal quality should be no less than 0.1. Table 2 shows that all four grids satisfy that criterion. The grid aspect ratio of a cell is the ratio between its longest and shortest edges. The maximum grid aspect ratio for each mesh is reported in Table 2. Optimally, this ratio should be below 20 but can be as high as 30 [5]. All four grids have maximums below 30 and it decreases to the desired range as the mesh is refined.

In this work, a simulation for each of the four grids was run for 10,000 iterations using Ansys Fluent. These simulations were performed on one node that employs two AMD EPYC 7513 32-Core processors and 1 TB of RAM. The time for each simulation to complete 10,000 iterations ($t_{comp,k}$) is included in Table 2. Table 2 shows that the simulation time increased by a factor of 3.1 as the number of meshes increased by a factor of 4.2.

2.2 Simulation Models and Assumptions

Ansys Fluent uses the finite volume method to numerically solve the relevant fluid flow and thermal transport partial differential equations. The volume of elements inside the supply and return ducts, the light bulbs, and the room region between the racks and room walls were modeled as air using the ideal gas assumption. The packages were modeled as solid Celotex insulation, and the light stems as solid steel. Table 3 contains

the material properties for those used to simulate the staging room. Note that the density, ρ, for air is a pressure and temperature dependent ideal gas with a reference density of ρ = 1.2 kg/m^3. The thermal conductivity, k, of Celotex is temperature dependent and the specific heat, c_p, is direction-dependent.

Table 3: Material properties, T is temperature in Kelvin

Material	ρ [kg/m^3]	k [W/(m-K)]	c_p [J/(kg-K)]	μ [kg/(m-s)]
Air	1.2 (ideal gas)	0.0242	1006.43	1.7894e-05
Wood	2310	0.173	2310	-
Steel	8030	16.27	502.48	-
Celotex	278	Radial - .1251 Tangential - .055 Axial - 1	3.81(T)+142 (linear)	-

The walls of the rack tubing and the air conditioning duct were modeled as shell conduction zones. Shell conduction zones are used to simulate conduction heat transfer through thin boundaries like sheets and plates. The solver allows the 2D surface to represent a 3D solid element with conduction by artificially inserting cells between volumes. Because the wood pallets are lattice structures, they were modeled as porous media regions. Porous media regions are used to represent permeable materials in which there is fluid flow impeded or influenced by solid material. The pallet volume is assumed to be half wood and half air.

The thermal energy generated within the packages and the lights were distributed uniformly within those structures using volumetric heat generation. Each light generated 100 W and each package generated 19 W, which is the maximum heat generation of each component. Each package has a surface emissivity of ε_{pg} = 0.21, while all other surfaces have emissivity of 1. The outer walls, ceiling, and floors of the room are adiabatic. The ventilation duct inlet is specified as a mass flow inlet, which sets a uniform mass flux

across the face specified. The return duct outlet is specified as a pressure outlet that prevents flow from entering the boundary.

The simulations use the k-ω turbulence model for the turbulent air regions, the discrete ordinates radiation model for heat radiation, and the SIMPLE algorithm for pressure coupling. The air flow throughout a room like the one in Figs. 2 and 3 with the specified mass flow, thermal conditions and pressure conditions will vary with time and location. However, the simulations conducted in this work employ a steady time model.

The results obtained from the simulations can vary by iteration ($i = 1, 2, \ldots 10{,}000$), package number ($j = 1, 2, \ldots 640$), and mesh ($k = A, B, C, D$). To note these differences a subscript scheme is used. For the mass flow rate ($\dot{m}$), pressure (P), and temperature (T) at the inlet and outlet, the corresponding letter is used with the first subscript used being the location (in or out, respectively) followed by an iteration symbol and then a mesh symbol. A bar over the letter ($\bar{\square}$) represents an iteration-averaged result from the last 5,000 iterations, in which case the iteration subscript is dropped. A delta symbol (Δ) before the results signifies that the result is the difference between the result and the results at the inlet.

A similar scheme is used for package temperatures. However, a subscript for the package number is used in between the subscripts for iteration and mesh and instead of the location subscript, an average (T_{avg}) or maximum (T_{max}) notes whether the result is the surface average or surface maximum temperature of an individual package. If the result represents the maximum or average of all 640 packages, the package number

subscript will be removed. The subscript $PGmax$ is used to represent the mean maximum temperature for all 640 packages.

3 Results

For each mesh *k = A, B, C, and D* evaluated over iteration $i = 1 - 10{,}000$, the simulation reports the outlet mass flow rate $\dot{m}_{out,i,k}$, the inlet and outlet static pressures, respectively, $P_{in,i,k}$ and $P_{out,i,k}$, and the outlet bulk temperature $T_{out,i,k}$. Additionally, for each package $j = 1 - 640$, the simulation reports the maximum and average surface temperature, respectively, $T_{max,i,j,k}$ and $T_{avg,i,j,k}$. These results were used as key metrics to evaluate mesh sensitivity and the model's ability to produce realistic results. Visual contours can be used to compare with the results to check the model for adherence to expected thermal and fluid behavior.

3.1 Inlet and Outlet Mass Flow Rate and Pressure Difference

Described below are the simulation results for the mass flow rate, $\dot{m}_{out,i,k}$ and pressure difference of the outlet from the inlet described as $\Delta P_{i,k} = P_{out,i,k} - P_{in,i,k}$.

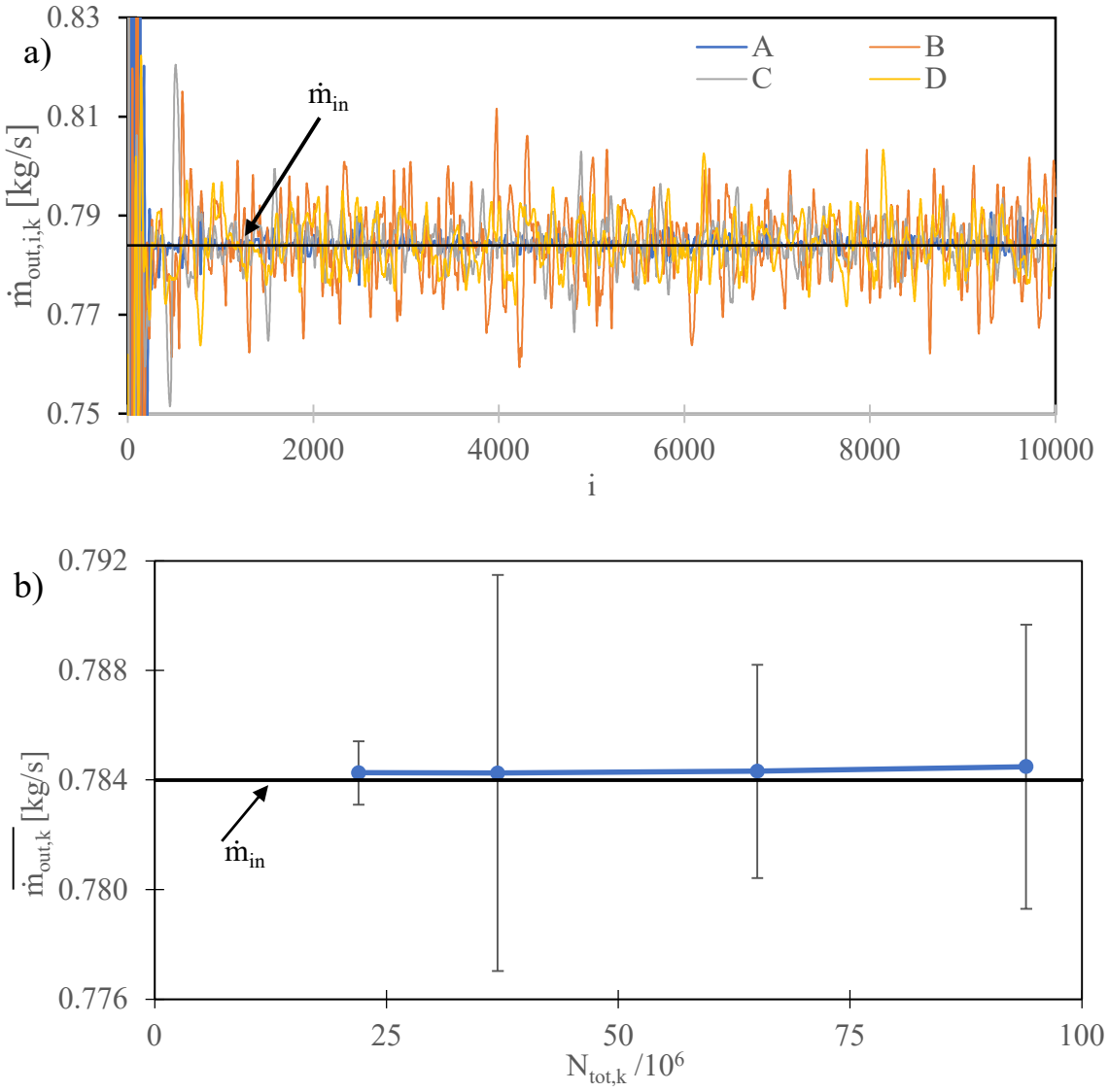

Figure 3: Inlet and outlet mass flow rates for all four meshes considered in this work. a) Outlet mass flow rate versus iteration, b) Iteration-averaged mass flow rate with two standard deviations over the last 5,000 iterations versus element count.

Figure 3a shows the simulated results for $\dot{m}_{out,i,k}$ for all four meshes, k for all 10,000 iterations, i. Also shown is the specified $\dot{m}_{in}$ marked by a horizontal black line. It can be seen that $\dot{m}_{out,i,k}$ oscillates randomly around $\dot{m}_{in}$ for all four grids. These oscillations for $i < 200$, vary significantly in amplitude, but settle closely around $\dot{m}_{in}$ for $i > 1{,}000$. The expected behavior of $\dot{m}_{out,i,k}$ is expected to follow the law of mass

conservation in which $\dot{m}_{out,i,k}$ is equal to the specified inlet mass flow rate $\dot{m}_{in}$. These results indicate that the $\dot{m}_{out,i,k}$ does not report the same rate for every iteration and vary slightly from $\dot{m}_{in}$.

Figure 3b shows the iteration-averaged mass flow rate, $\overline{\dot{m}_{out,k}}$, results from $i = 5{,}001$ to $10{,}000$ graphed against $N_{tot,k}$ for all four meshes. Two standard deviations, $2\sigma_{\dot{m}_{out,k}}$, of the outlet mass flow rate are represented by the error bars on each symbol and give the statistical 95% confidence interval from the last 5,000 iterations. $\dot{m}_{in}$ is shown by the horizontal black line. Each of the four meshes report a $\overline{\dot{m}_{out,k}}$ that is slightly higher than the specified $\dot{m}_{in}$. The equations use to calculate $\overline{\dot{m}_{out,k}}$ and $2\sigma_{\dot{m}_{out,k}}$ are shown in Equation 1.

$$\overline{\dot{m}_{out,k}} = \frac{\sum_{i=5,001}^{10,000} \dot{m}_{out,k,i}}{5{,}000},\ \sigma^2_{\dot{m}_{out,k}} = \frac{\sum_{i=50}^{10,000} \left(\dot{m}_{out,i,k} - \overline{\dot{m}_{out,k}}\right)^2}{4{,}999} \quad \{1\}$$

Table 4: Iteration-averaged, difference from inlet, and standard deviation of mass flow rate results

Mesh, k	$\overline{\dot{m}_{out,k}}$ [kg/s]	$\frac{\overline{\Delta\dot{m}_{out,k}}}{\dot{m}_{in}}$	$2\sigma_{\dot{m}_{out,k}}$ [kg/s]	$\frac{2\sigma_{\dot{m}_{out,k}}}{\dot{m}_{in}}$
A	0.78426	0.033%	0.002	0.30%
B	0.78425	0.032%	0.014	1.84%
C	0.78432	0.040%	0.008	0.99%
D	0.78449	0.062%	0.010	1.32%

For further analysis, Table 4 presents the numerical value of $\overline{\dot{m}_{out,k}}$, the relative difference of the difference of the mass flow rate between the outlet and the inlet and the inlet mass flow rate, $\frac{\overline{\Delta\dot{m}_{out,k}}}{\dot{m}_{in}}$ where $\overline{\Delta\dot{m}_{out,k}} = \overline{\dot{m}_{out,k}} - \dot{m}_{in}$, the numerical value of

$2\sigma_{\dot{m}_{out,k}}$, and the relative difference of two standard deviations and the inlet mass flow rate, $\frac{2\sigma_{\dot{m}_{out,k}}}{\dot{m}_{in}}$.

From the results presented, the simulation reports a $\dot{m}_{out,i,k}$ that oscillates with iteration slightly different from $\dot{m}_{in}$ for each mesh but when the iteration-averaged, $\overline{\dot{m}_{out,k}}$, is considered, the simulation is reporting just above the specified $\dot{m}_{in}$ but is well within $2\sigma_{\dot{m}_{out,k}}$ for each mesh. This result indicates the simulations, and each mesh, produce results close to what is expected. Table 4 shows that $\frac{\overline{\Delta\dot{m}_{out,k}}}{\dot{m}_{in}}$ is far smaller than $\frac{2\sigma_{\dot{m}_{out,k}}}{\dot{m}_{in}}$, meaning that the deviation due to iteration is higher than the deviation from the iteration-averaged results and the specified mass flow rate. Variation due to iteration is unavoidable and does not decrease with mesh refinement. With the variation due to iteration being higher than the variance from the expected result, one can conclude that simulation needs no further refinement.

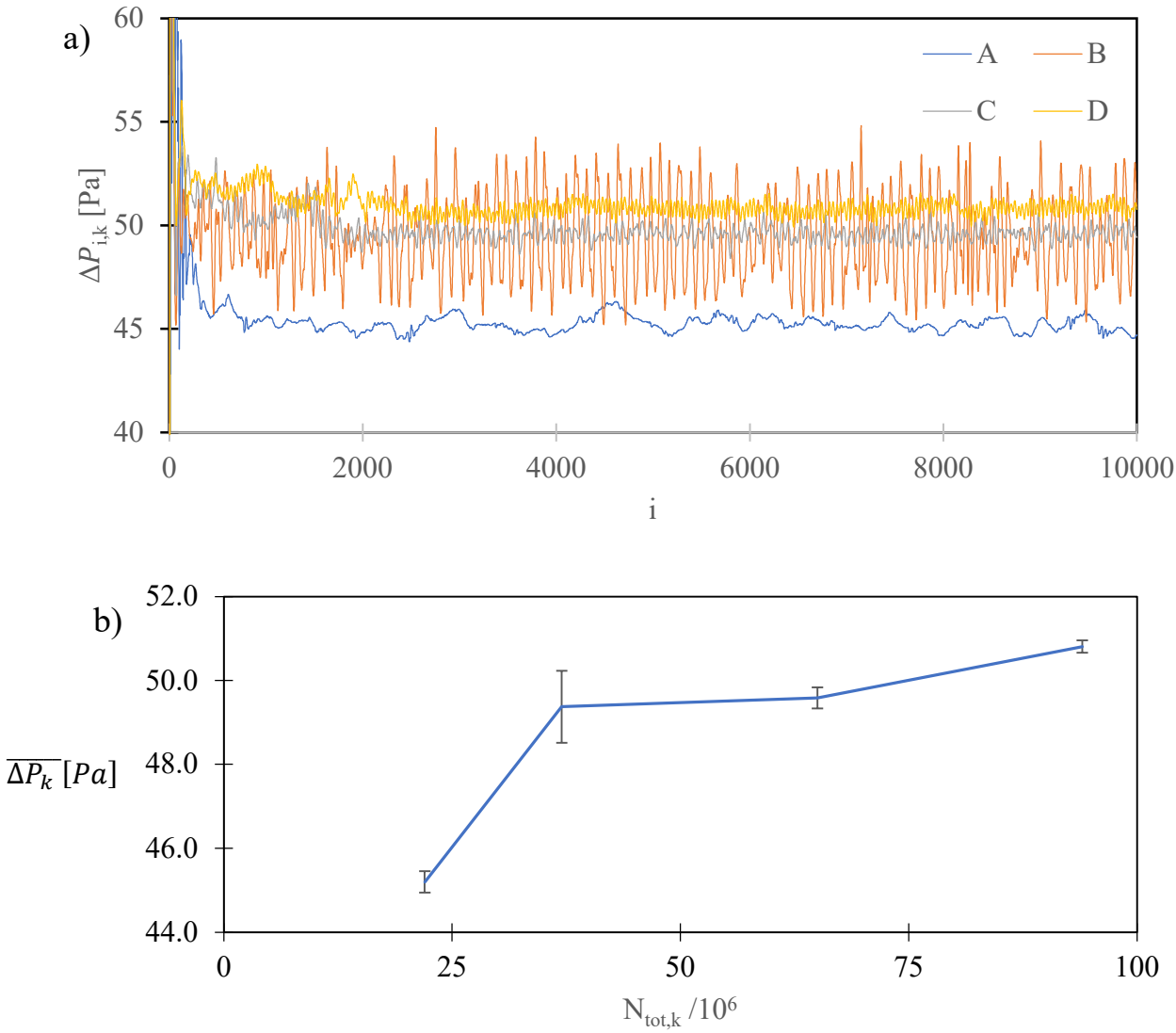

Figure 4: Outlet minus inlet pressure for all four meshes considered in this work. a) Pressure difference versus iteration, b) Iteration-averaged pressure difference with two standard deviations over the last 5,000 iterations versus element count.

Figure 4a is a graph of the static pressure difference between the domain outlet and inlet, $\Delta P_{i,k}$, versus iteration. For all four meshes, for $i < 2000$, the pressure difference varies more with iteration than it does for $i > 2000$. For $i > 2000$, the pressure difference versus iteration varies randomly about constant values that are different for each mesh. The magnitude of the variations for Mesh B is larger than the

other meshes. The reason for this difference is not currently understood. The symbols connected by straight lines in Figure 4b show the average pressure difference for the last 5,000 iterations for each mesh, $\overline{\Delta P_k}$ versus $N_{tot,k}$. The error bars show two standard deviations of those results, $2\sigma_{\Delta P_k}$. Figure 4b shows that the average pressure difference increases more than the standard deviation as the mesh count increases from $N_{tot} = 23$ to 97 million elements. However, the increase is less significant as the mesh is further refined. We conclude that the pressure difference may continue to change somewhat with further mesh refinement. Future work may consider plotting stagnation instead of static pressure differences. Equation 2 shows how $\overline{\Delta P_k}$ and $2\sigma_{\Delta P_k}$ are calculated.

$$\overline{\Delta P_k} = \frac{\sum_{i=5,001}^{10,000} \Delta P_{k,i}}{5{,}000}, \quad \sigma^2_{\Delta P_k} = \frac{\sum_{i=5,001}^{10,000} \left(\Delta P_{i,k} - \overline{\Delta P_k}\right)^2}{4{,}999} \qquad \{2\}$$

3.2 Air Outlet and Package Temperatures

The results presented in this section focus on the outlet temperature, $T_{out,i,k}$, and the global average and maximum surface temperature of all 640 packages, $T_{avg,i,k}$ and $T_{max,i,k}$ respectively. The calculation for these results is shown in Equation 3.

$$T_{max,i,k} = \max_{all\ j} T_{max,i,j,k}, \quad T_{avg,i,k} = \frac{\sum_{j=1}^{640} T_{avg,i,j,k}}{640} \qquad \{3\}$$

Like the previous section, results from the simulation are examined for each mesh for $i = 1\ to\ 10{,}000$. The outlet temperature can be predicted using the conservation of energy. In these simulations, the inlet mass flow rate $\dot{m}_{in}$, total package and lighting heat generation rate $\dot{Q}_{tot}$, air specific heat c_p, and inlet temperature T_{in} are specified and constant. Because the walls are adiabatic, the expected outlet air temperature may be calculated based on conservation of energy as shown in Equation 4. In lieu of having an expected average and maximum package temperature, the results of the less refined meshes are compared with the results from the most refined mesh, mesh D.

$$T_{out,EB} = \frac{\dot{Q}_{tot}}{\dot{m}_{in} c_p} + T_{in} = 34.196℃ \qquad \{4\}$$

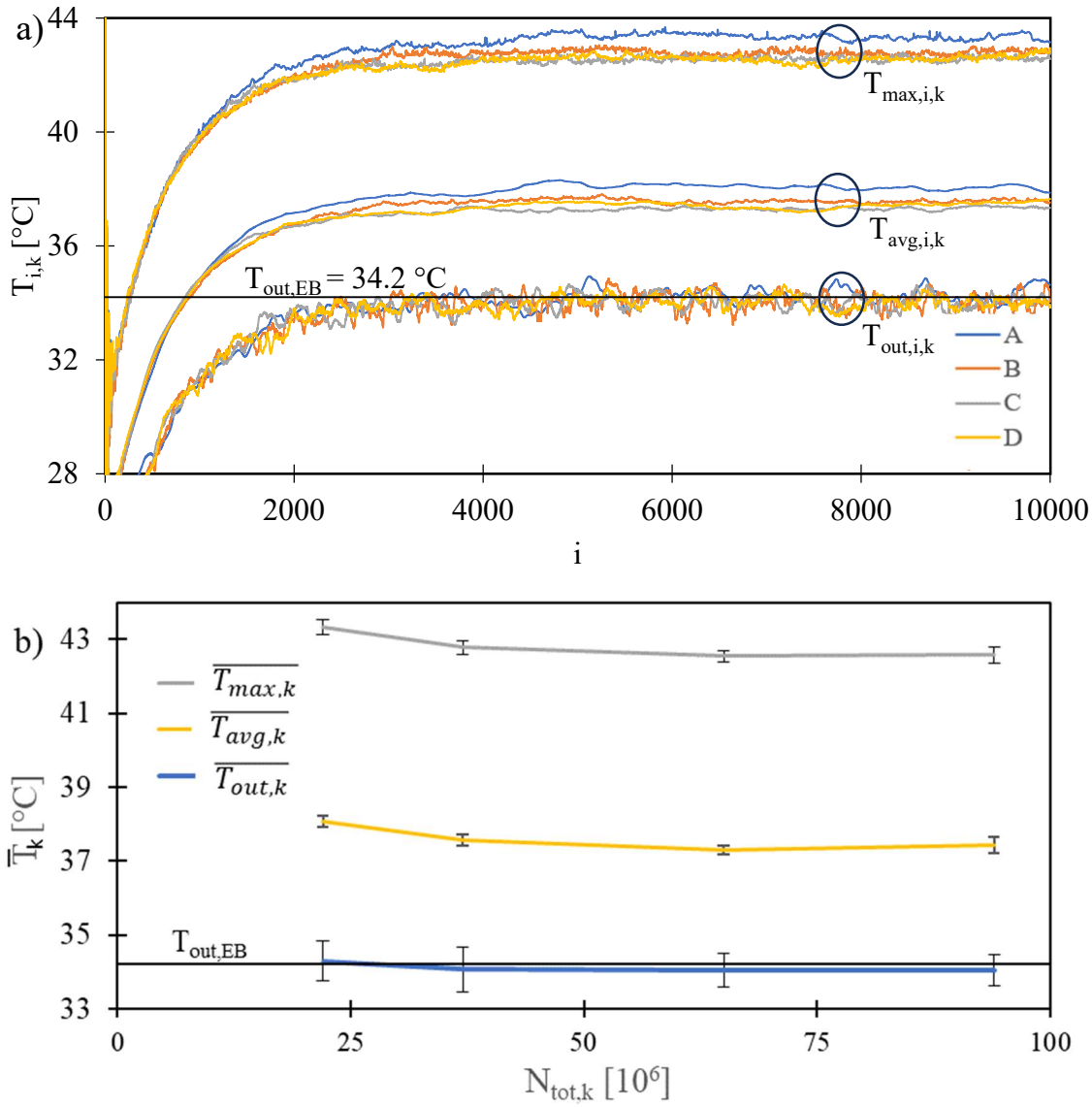

Figure 5: a) Outlet temperature and average and maximum package surface temperatures for all four meshes. a) Temperature versus iteration b) Average temperature with two standard deviations over the last 5,000 iterations versus element count

Figure 5a shows the outlet air $T_{out,i,k}$ and global package surface average $T_{avg,i,k}$ and maximum $T_{max,i,k}$ temperatures against $i = 1 - 10{,}000$ for the four computational meshes. For all meshes, the three temperatures increase from an initial value with iteration for i < 4,000. $T_{out,EB}$ is shown by a black line, and may be compared to the simulated outlet values, $T_{out,i,k}$. It can be observed that the values of $T_{out,i,k}$ from all four

meshes vary about $T_{out,EB}$. Similarly, the values of $T_{max,i,k}$ and $T_{avg,i,k}$ are similar across all four meshes but vary independently by iteration.

Figure 5b takes an iteration-average approach for the values of $T_{out,i,k}$, $T_{avg,i,k}$, and $T_{max,i,k}$ which is achieved by averaging over the last 5,000 iterations (from $i = 5{,}001 - 10{,}000$) as shown in Equation 5 to produce $\overline{T_{out,k}}$, $\overline{T_{avg,k}}$, and $\overline{T_{max,k}}$ and plots them against $N_{tot,k}$. Two standard deviations for each result, $2\sigma_{T_{out,k}}$, $2\sigma_{T_{avg,k}}$, and $2\sigma_{T_{max,k}}$, are shown with black error bars from the last 5,000 iterations which are calculated using Equation 6. Across all three temperatures, Mesh A reports a higher temperature than the other three more refined grids.

$$\overline{T_{out,k}} = \frac{\sum_{i=5,001}^{10,000} T_{out,i,k}}{4{,}999}, \overline{T_{avg,k}} = \frac{\sum_{i=5,001}^{10,000} T_{avg,i,k}}{5{,}000}, \overline{T_{max,k}} = \frac{\sum_{i=5,001}^{10,000} T_{max,i,k}}{5{,}000} \quad \{5\}$$

$$\sigma^2_{T_{out,k}} = \frac{\sum_{i=5,001}^{10,000} \left(T_{out,i,k} - \overline{T_{out,k}}\right)^2}{4{,}999} \; \sigma^2_{T_{avg,k}} = \frac{\sum_{i=5,001}^{10,000} \left(T_{avg,i,k} - \overline{T_{avg,k}}\right)^2}{4{,}999},$$

$$\sigma^2_{T_{max,k}} = \frac{\sum_{i=5,001}^{10,000} \left(T_{max,i,k} - \overline{T_{max,k}}\right)^2}{4{,}999} \quad \{6\}$$

Table 5: Outlet temperature, deviation, and comparison to energy balance

Mesh, k	$\overline{T_{out,k}}$ [°C]	$\frac{\overline{\Delta T_{out,k}} - \Delta T_{out,EB}}{\Delta T_{out,EB}}$	$2\sigma_{T_{out,k}}$ [°C]	$\frac{2\sigma_{T_{out,k}}}{\Delta T_{out,EB}}$
A	34.29	0.58%	0.54	3.25%
B	34.07	-0.79%	0.61	3.72%
C	34.05	-0.91%	0.44	2.70%
D	34.05	-0.89%	0.43	2.60%

Table 5 presents the results from the four meshes of $\overline{T_{out,k}}$, the relative difference of the difference of difference of the outlet temperature from the inlet temperature, $\overline{\Delta T_{out,k}} = \overline{T_{out,k}} - T_{in}$, and the expected difference from energy balance, $\frac{\overline{\Delta T_{out,k}} - \Delta T_{out,EB}}{\Delta T_{out,EB}}$, two standard deviations of the last 5,000 iterations, and the relative difference of two

standard deviations and the expected difference from energy balance, $\frac{2\sigma_{T_{out,k}}}{\Delta T_{out,EB}}$. The difference from the inlet is used because it provides a scaling to the results that allows the true differences to be examined.

From these results it can be shown that Mesh A over predicts the temperature expected from energy balance while the three other grids under predict it. Four all four grids the relative difference from the iteration-averaged results, $\frac{\overline{\Delta T_{out,k}}-\Delta T_{out,EB}}{\Delta T_{out,EB}}$, is lower in magnitude than the relative difference from standard deviation of iteration, $\frac{2\sigma_{T_{out,k}}}{\Delta T_{out,EB}}$. This means, like the mass flow rate, that the outlet temperature from each mesh has variation due to iterating than the variation from the expected outlet temperature.

Table 6: Average package surface temperature, deviation, and comparison to Mesh D

Mesh, k	$\overline{T_{avg,k}}$ [°C]	$\overline{T_{avg,k}} - \overline{T_{avg,D}}$ [°C]	$\frac{\overline{T_{avg,k}} - \overline{T_{avg,D}}}{\overline{\Delta T_{avg,D}}}$	$2\sigma_{T_{avg,k}}$ [°C]	$\frac{2\sigma_{T_{avg,k}}}{\overline{\Delta T_{avg,k}}}$
A	38.07	0.64	3.27%	0.15	0.74%
B	37.57	0.14	0.73%	0.14	0.69%
C	37.31	-0.12	-0.61%	0.11	0.55%
D	37.43	-	-	0.21	1.08%

Table 7: Maximum package surface temperature, deviation, and comparison to Mesh D

Mesh	$\overline{T_{max,k}}$ [°C]	$\overline{T_{max,k}} - \overline{T_{max,D}}$ [°C]	$\frac{\overline{T_{max,k}} - \overline{T_{max,D}}}{\overline{\Delta T_{max,D}}}$	$2\sigma_{T_{max,k}}$ [°C]	$\frac{2\sigma_{T_{max,k}}}{\overline{\Delta T_{max,k}}}$
A	43.35	0.77	3.09%	0.20	0.80%
B	42.79	0.21	0.83%	0.19	0.77%
C	42.56	-0.02	-0.08%	0.15	0.61%
D	42.58	-	-	0.23	0.95%

Tables 6 and 7 present similar data to those presented in Table 5, except instead of comparing temperature values relative to energy balance, the temperatures are compared

relative to the results from Mesh D, and the standard deviation is compared to their respective results. Table 6 and 7 show that Mesh A and D have the largest disagreement. Mesh B, C, and D report similar results but Mesh C is much closer on both accounts. Mesh B and C vary from Mesh D in a similar magnitude to how they vary with iteration (i.e. $\frac{\overline{T_{avg,k}}-\overline{T_{avg,D}}}{\overline{\Delta T_{avg,D}}} \approx \frac{2\sigma_{T_{avg,k}}}{\overline{\Delta T_{avg,k}}}$ and $\frac{\overline{T_{max,k}}-\overline{T_{max,D}}}{\overline{\Delta T_{max,D}}} \approx \frac{2\sigma_{T_{max,k}}}{\overline{\Delta T_{max,k}}}$).

For both the average and maximum surface temperatures, all grids report a similar temperature. However, Grid A reports slightly higher than the three more refined grids which intersect one another. Outlined in 10 CFR 72, the maximum exposed surface temperature of a package must be below 50°C. All the grids report the maximum package surface temperatures that are at least 6.6°C below the maximum allowable. These results predict that there would be 6.4°C a margin between the maximum package surface temperature in a fully loaded room when accounting for two standard deviations over iteration, with all packages generating the maximum allowable heat, and the allowed design limit.

Of the five quantities presented in Figs. 3, 4 or 5, none of them become constant (independent of iteration) for any of the four meshes, even after 10,000 iterations. However, all five become quasi-constant after i = 5,000 iterations, in that they vary randomly about different mean values that to appear to be independent of iteration. Moreover, the magnitudes of the variations also appear to be independent of iteration.

3.3 Spatial Variation of Air Velocity and Temperature and Package Surface Temperature in the Mostly Highly Refined Mesh

In this section, visual representations from the simulation of Mesh D at $i = 10{,}000$ are evaluated and examined to investigate the flow pattern and temperature of the room and how that affects the temperature distribution of the packages based upon their location in the room.

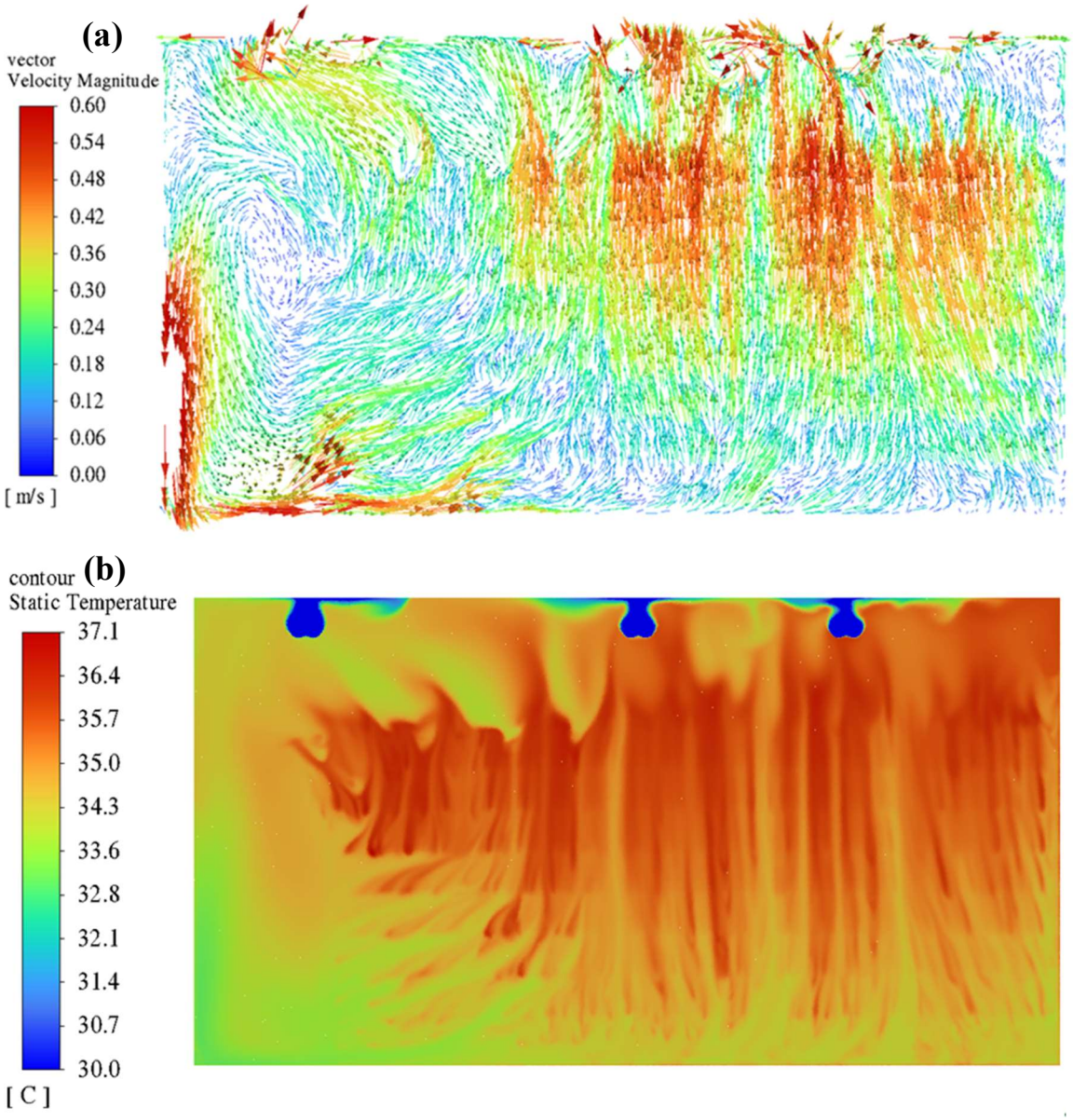

Figure 6: Spatial variation of air properties in the vertical plane bisecting the gap separating racks 2 and 3. (a) velocity direction and amplitude. (b) temperature.

Figure 6 shows the spatial variation of air properties in the vertical plane bisecting the gap separating Racks 2 and 3. Fig. 6a exhibits vectors whose orientation show the air direction, and whose amplitude and color show the air speed. Air speeds greater than 0.6 m/s, in the proximity to the diffusers, are suppressed to better exhibit the velocities lower in the room. Figure 6b is a contour plot of the air temperature. Temperatures below 30°C, near the diffusers, are also suppressed to better show temperature variations lower in the room.

Figure 6 shows that relatively cool air moves to the open region near the front of the room as it drops from the diffusers. The air is heated by the packages and drifts upward, assisted by buoyancy, within the shelves. The highest velocities in the plane (excluding the region near the diffusers) is at the lower front of the room, where it is drawn into the shelves, and in the middle of the racks. The highest temperature is also among the racks.

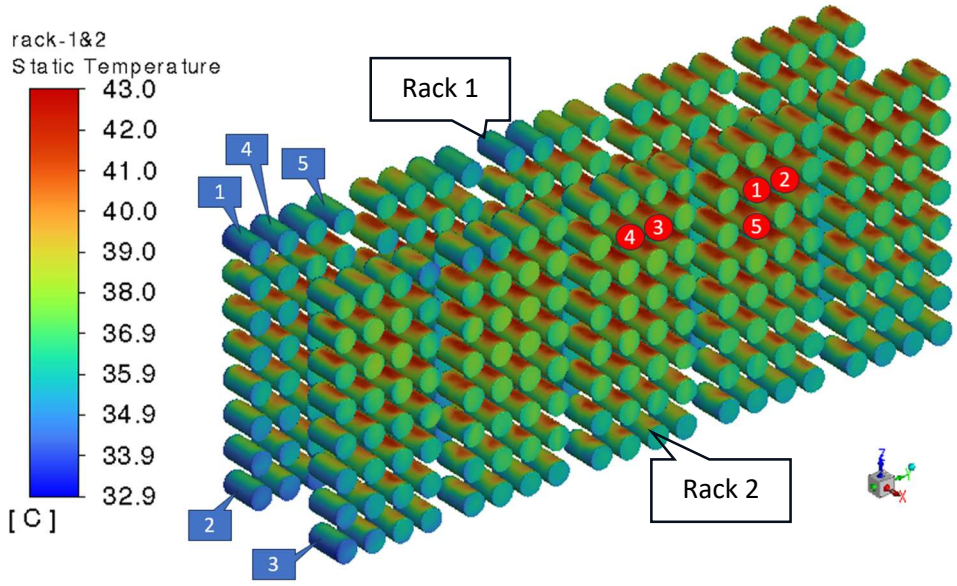

Figure 7: Rack 1 and 2 package surface temperature contours from Mesh D simulation at $i = 10,000$. The locations of the packages with the five coldest (blue) minimum and five hottest (red) maximum surface temperatures are indicated.

Figure 7 is a perspective view of the surface temperature contours on the 320 packages located in Racks 1 and 2. The packages of Racks 3 and 4 are removed to allow the figure to show the hottest region. The temperature patterns in Racks 3 and 4 are nearly mirror images of Racks 1 and 2. They are slightly different because, while the air delivery diffusers are near the center of the ceiling, the return duct is above Rack 4.

In Fig. 7, the locations of the five packages with the hottest maximum surface temperatures are identified by red circles. They are all located in Rack 2 in bays 3 and 4 on levels 6 and 7, and their maximum temperatures are between 42.05°C and 42.37°C. The locations of the five packages with the lowest maximum temperatures are shown using blue rectangles. They are at the top and bottom of Racks 1 and 2, near the front of the room, and their temperatures range between 39.12 and 39.72°C. The locations of the hottest and coldest packages are consistent with the air temperatures and flow patterns shown in Fig. 6. For experimental validation, these packages would be the best to sample temperatures using thermocouples to compare with the results from these simulations.

3.4 Package Temperature Comparisons with Less Refined Mesh Results

As the previous section focused on the global average and maximum package surface temperature, this section focuses on the difference for individual packages. Since the surface temperatures slightly fluctuate with iteration, an iteration-average for $T_{max,i,j,k}$ is achieved is achieved by averaging the maximum surface temperature for each package, j, over iterations, $i = 5{,}001\ to\ 10{,}000$, as shown in Equation 7.

$$\overline{T_{max,J,k}} = \frac{\sum_{i=5,001}^{10,000} T_{max,i,j,k}}{5{,}000} \quad \{7\}$$

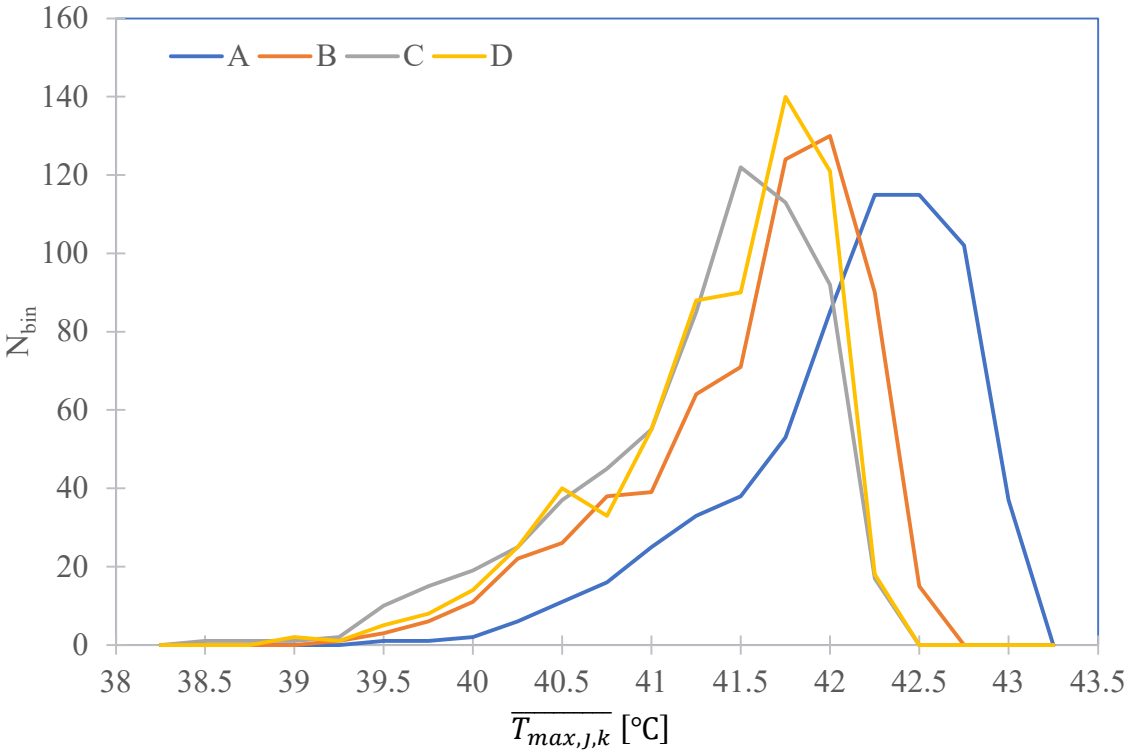

Figure 8: Distributions of the iteration-averaged maximum package surface temperature for all four meshes.

Figure 8 shows the distribution of iteration-averaged, maximum surface temperatures for all 640 packages, $\overline{T_{max,J,k}}$ for the four meshes, k. $\overline{T_{max,J,k}}$ was sorted into bins of 0.25°C. The number of packages in each bin, N_{bin}, is shown on the y-axis. $\overline{T_{max,J,k}}$ varies from 38.5°C to 43.25°C for all four meshes, with most packages showing

a right-leaning distribution, meaning that most packages have a maximum surface temperature that is closer to the warmer end of the temperature range.

Table 8: Mean and standard deviation of the maximum package surface temperatures for all four mesh simulations.

Mesh, k	$\overline{T_{PGmax,k}}$ [°C]	$2\sigma_{T_{PGmax,k}}$ [°C]	$\frac{2\sigma_{T_{PGmax,k}}}{\overline{\Delta T_{PGmax,k}}}$
A	42.22	1.29	5.03%
B	41.67	1.28	5.10%
C	41.39	1.33	5.35%
D	41.49	1.24	4.99%

Table 8 contains the mean of the iteration-averaged, maximum surface temperature of all 640 packages, $\overline{T_{PGmax,k}}$, two standard deviations of the iteration-averaged, maximum surface temperature of all 640 packages, $2\sigma_{T_{PGmax,k}}$, and the relative difference of two standard deviations and the difference between the mean and the inlet temperature, $\frac{2\sigma_{T_{PGmax,k}}}{\overline{\Delta T_{PGmax,k}}}$. The calculations used to generate the mean, mean difference, and standard deviation can be found in Equations 8 and 9.

Figure and Table 8 show that like the global variables, the maximum surface temperature for the packages are reported higher in Mesh A than the three other meshes. Meshes B and C have very similar distributions to Mesh D, with Mesh B slightly higher and Mesh C slightly less. The means, $\overline{T_{PGmax,k}}$, of the three most refined meshes are close to one another. The deviation and the relative difference of the deviation, $2\sigma_{T_{PGmax,k}}$ and $\frac{2\sigma_{T_{PGmax,k}}}{\overline{\Delta T_{PGmax,k}}}$, are similar for all four meshes which indicate that the simulations sufficiently provide the range and distribution at the mesh sizes investigated.

$$\overline{T_{PGmax,k}} = \frac{\sum_{j=1}^{640} \overline{T_{max,J,k}}}{640}, \overline{\Delta T_{PGmax,k}} = \overline{T_{PGmax,k}} - T_{in} \quad \{8\}$$

$$\sigma^2_{T_{PGmax,k}} = \frac{\sum_{i=1}^{640} \left(\overline{T_{max,J,k}} - \overline{T_{PGmax,k}}\right)^2}{640} \quad \{9\}$$

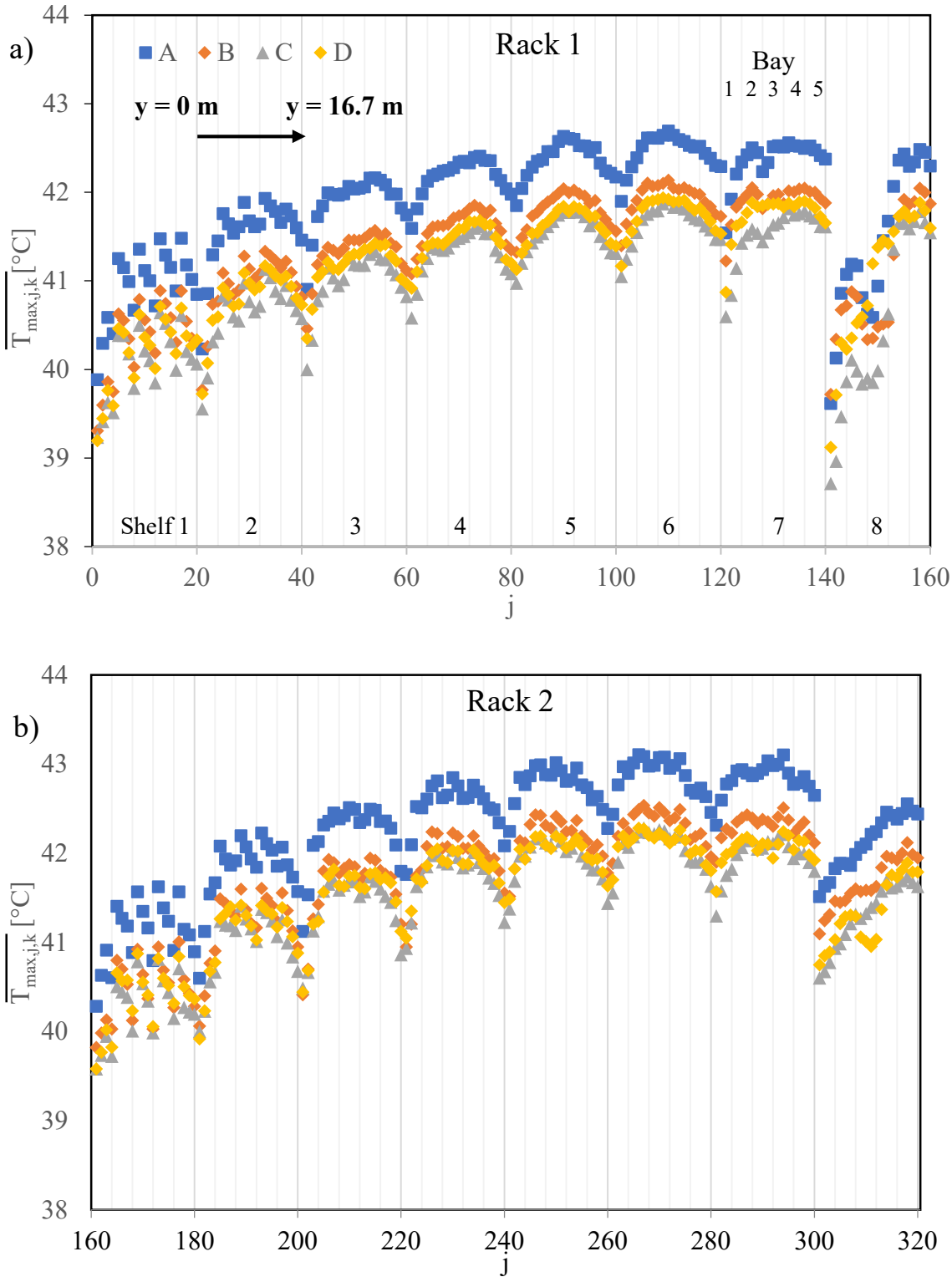

Figure 9: Maximum package surface temperature versus linearized location for all four mesh simulations. (a) Rack 1. (b) Rack 2.

Figure 9 shows $\overline{T_{max,J,k}}$ against the package index, j, in Racks 1 and 2. Racks 3 and 4 are omitted because they report near mirror $\overline{T_{max,J,k}}$ to Racks 2 and 1, respectively. The package index number, j, starting at package 1 in Rack 1 on the first shelf in the first bay closest to the front of the room increase by one as they progress in the y-direction along the shelf level, increase by 20 for each shelf level from first shelf, and by 160 for each rack. Shelves are indicated by the bolded major vertical gridlines and bays by the minor vertical gridlines. In the racks, $\overline{T_{max,J,k}}$ increases with shelf level up to shelf 6, stabilize for shelf 7, and decrease in shelf 8. In general inside each shelf, $\overline{T_{max,J,k}}$ increases and then decreases as the packages progress towards the back of the room, peaking in bays 3 and 4. This further verifies the fluid and temperature behavior in Figures 6 and 7 where temperatures are higher on the shelves 6 and 7 and bays 2, 3, and 4 where natural convection drives the flow and temperatures are lower in bay 1 and shelf 8 where the flow is driven by forced convection.

The four meshes show a lot of disagreement in Shelf 8 on Rack 1. This phenomenon is also noted on Rack 4. This is believed to be caused by the higher air velocities from the diffusers that blow across the surfaces of those packages. These figures also show a similar phenomenon seen previously in the global results and in the package temperature distributions with Mesh A reporting a $\overline{T_{max,J,k}}$ higher than the other three more refined meshes. It should be noted that $\overline{T_{max,J,k}}$ although different in magnitude for the four meshes, follows a similar pattern against package index.

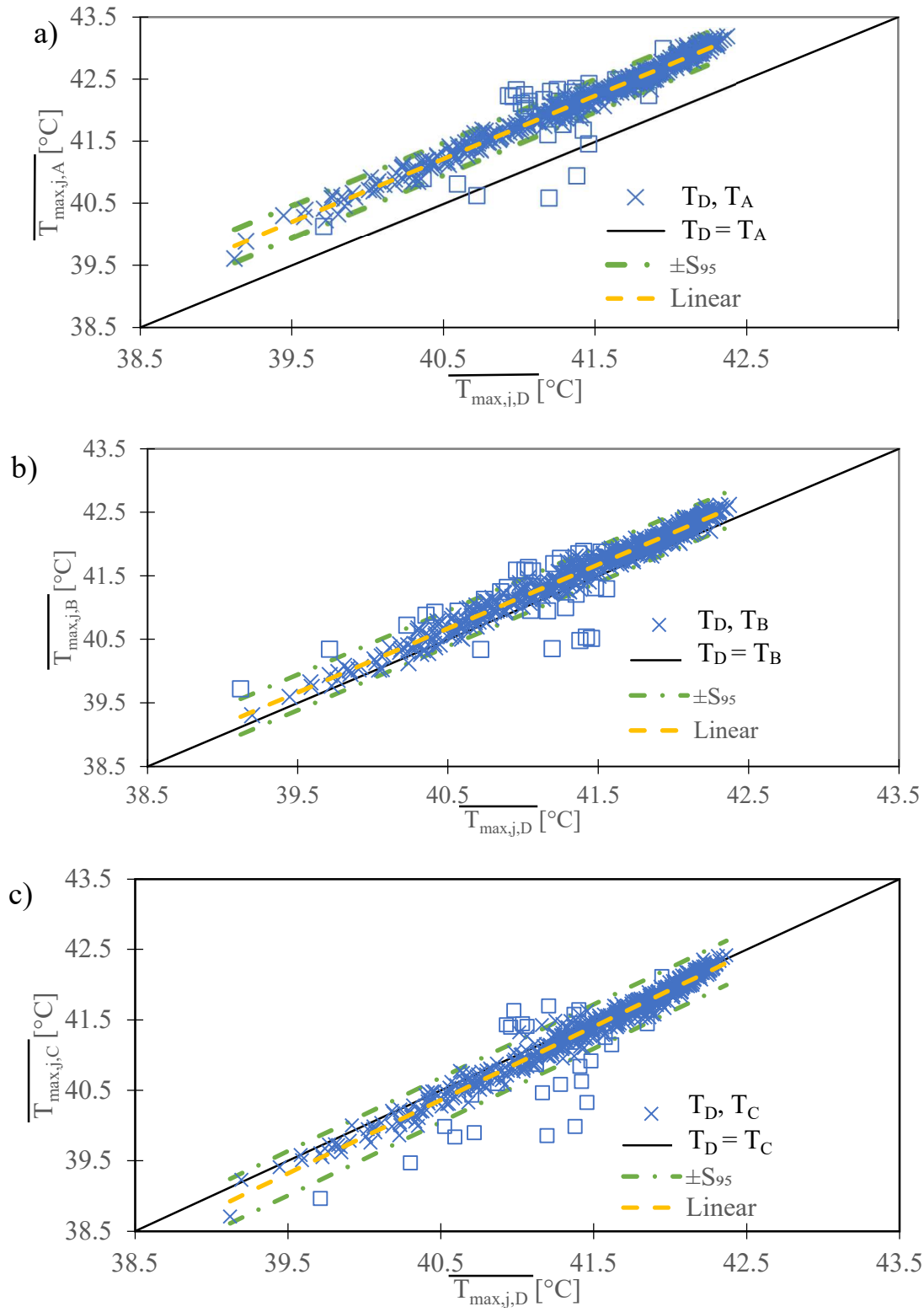

Figure 10: Individual maximum package surface temperature from less refined mesh simulations versus result from Mesh D (most refined). Comparisons between Mesh a) A and D, b) B and D, and c) C and D.

Figure 10 shows a package-to-package comparison for $\overline{T_{max,J,k}}$ between the less-refined meshes and Mesh D. The blue x's note the data comparison between meshes, the black line is a one-to-one, the dashed yellow line is the linear fit of all package comparisons, and the green dashed lines represent two standard error of estimates, $\pm 2S_k$. The blue boxes are the data comparisons for the forty packages located on the eighth shelf in Racks 1 and 4.

Table 9: Linear-fit statistics between individual maximum package temperatures from Mesh D and from less refined meshes.

Mesh, k	m_k	$\overline{T_{PGmax,k}} - \overline{T_{PGmax,D}}$ [°C]	$2S_k$[°C]	$2S_{exc,k}$ [°C]
A	1.177	0.73	0.259	0.143
B	1.006	0.18	0.280	0.169
C	1.042	-0.09	0.314	0.179

Table 9 shows the slope of the fitted lines in Figure 10, m_k, the difference between the mean iteration-averaged, package maximum surface temperature for the less refined meshes and Mesh D, $\overline{T_{PGmax,k}} - \overline{T_{PGmax,D}}$, and two standard error of estimates for the data comparisons in Figure 10 with and without the forty packages located on the eighth shelf in Racks 1 and 4. The process for calculating the slope and standard error of estimate are in Equations 10, 11, and 12.

$$m_k = \sum_{j=1}^{640} \frac{(\overline{T_{max,J,D}} - \overline{T_{PGmax,D}})(\overline{T_{max,J,k}} - \overline{T_{PGmax,k}})}{(\overline{T_{max,J,D}} - \overline{T_{PGmax,D}})} \quad \{10\}$$

$$b_k = \overline{T_{PGmax,k}} - m_k(\overline{T_{PGmax,D}}) \quad \{11\}$$

$$S_k^2 = \frac{\sum_{j=1}^{640}[m_k\overline{T_{max,J,D}} + b_k - \overline{T_{max,J,k}}]^2}{638} \quad \{12\}$$

Figure 10 and Table 9 show that Mesh A reports 0.73°C higher maximum surface temperatures for the packages than Mesh D. Mesh B reports much closer with 0.18°C being the mean difference. Mesh C under reports 0.09°C less on average than Mesh D.

Mesh B is the closest to a one-to-one relationship and Mesh A is the furthest, which is deduced from the difference between m_k and 1. $2S_k$ is much lower when not considering the packages in the top shelf of Racks 1 and 4.

From the confirmations and verifications discussed previously in this section, it can be inferred that Mesh A is not adequate to report accurate package temperatures. From the data, Meshes B and C report temperatures similar to the most refined Mesh, but Mesh B shows larger variations with iterations than the two most refined Meshes. With that being the case, Mesh C is the best candidate for the application given it's similar performance with Mesh D, it's low iteration variance, and competitive computational time. From evaluating the number of iterations needed for the temperature results to converge, 7,000 iterations would be sufficient to report stabilized temperature results.

4 Conclusion

4.1 Discussion

In some situations, it is advantageous to store heat generating packages containing radiological materials in dense configurations. This work evaluated the thermal response of a staging room loaded with 640 packages generating the maximum allowable heat on pallets and racks using CFD software Ansys Fluent for the purpose of developing a predictive configurable model.

This work used previous insight to limit the number of shelves in the room and utilize the k-omega turbulence model and steady-state time-stepping. Four meshes were generated from the representative geometry and were evaluated on their ability to conserve mass and energy and reflect logical real world physics phenomena. It was found that each grid was able to properly conserve mass and energy at the inlet and outlet of the system.

Temperature results for the packages were compared for the four meshes. These results stabilized around the 4,000 iteration mark and oscillated randomly around a single value for 6,000 more iterations. The coarsest mesh, A, reported package temperatures that were higher than the ones reported for the other meshes. Mesh B reported similar temperatures as the other three grids but had a higher deviation in oscillations. To reduce the computational time needed to produce package temperatures in the predictive model while also maintaining results accurately represented by the finest mesh, it is recommended to use Mesh C ran to 7,000 iterations.

Along with the evaluation of mesh efficiency, the physics phenomenon was observed inside the room. The simulations suggested that the cold air would be directed

to the top and then circulate in the room. Where the flow was the highest along the top shelves and towards the front of the room, packages showed lower surface temperatures. While packages that were located towards the middle of the racks had higher surface temperatures. The highest surface temperatures were found on rack 2 on shelves 6 and 7 in bays 3 and 4. The simulation also showed that velocities were higher near these packages where natural convection was highest. The air would circulate in the room until being pushed out the outlet duct. This behavior followed what would be expected for a room with packages in the given configuration.

4.2 Future Work

Continued efforts on the simulation of the thermal behavior of this hypothetical staging room should focus on the classification of the flow pattern in the room and the evaluation of the temperature oscillations in the room. Sampling of the Outlet Stagnation Pressure to investigate the differences in static pressure presented in this work. Simulations could be carried out with pseudo-transient time stepping models that would help evaluate if the temperature fluctuations follow a periodic pattern. Higher resolution (more mesh elements) could be used around the top packages and those located towards the front of the room to try and capture the flow fluctuations around the packages that showed high disagreement between mesh refinements i.e. in Racks 1 and 4.

In addition to software-to-software comparisons with another commercial CFD software, results should be experimentally evaluated by taking measurements using thermocouples and anemometers in a scale model. The packages that reported the highest and lowest temperatures would be some of the best packages to compare temperatures with. Anemometers could be used to evaluate the velocities in the room and compare

with data collected in the simulation. A thermal camera could also be used to compare the package temperature profiles with the ones presented in this paper.

References

[1] 10 CFR 71 Packaging and Transportation of Radiological Materials

[2] Savannah River National Laboratory, "Safety Analysis Report Model 9975." Savannah River Nuclear Solutions, LLC, Apr. 2014.

[3] Austin Flynt, "ESP-491 HVAC CFD Modeling: Phase 2 CFD Report." Jacobs Engineering, Mar. 10, 2020.

[4] STARCCM+. SIEMENS, Version 12.04.010.

[5] Joel Kaderka, "A Scoping Study to Develop a Computational Fluid Dynamics Based Model to Predict Radiological Materials Packaging Temperatures within a Generic Staging Building," University of Nevada, Reno. May. 2021.

[6] "ANSYS FLUENT 12.0 User's Guide." Ansys

[7] Solidworks. Dassault Systems, Version 2021.

Appendix

A1. Temperature Contour of Rack 1

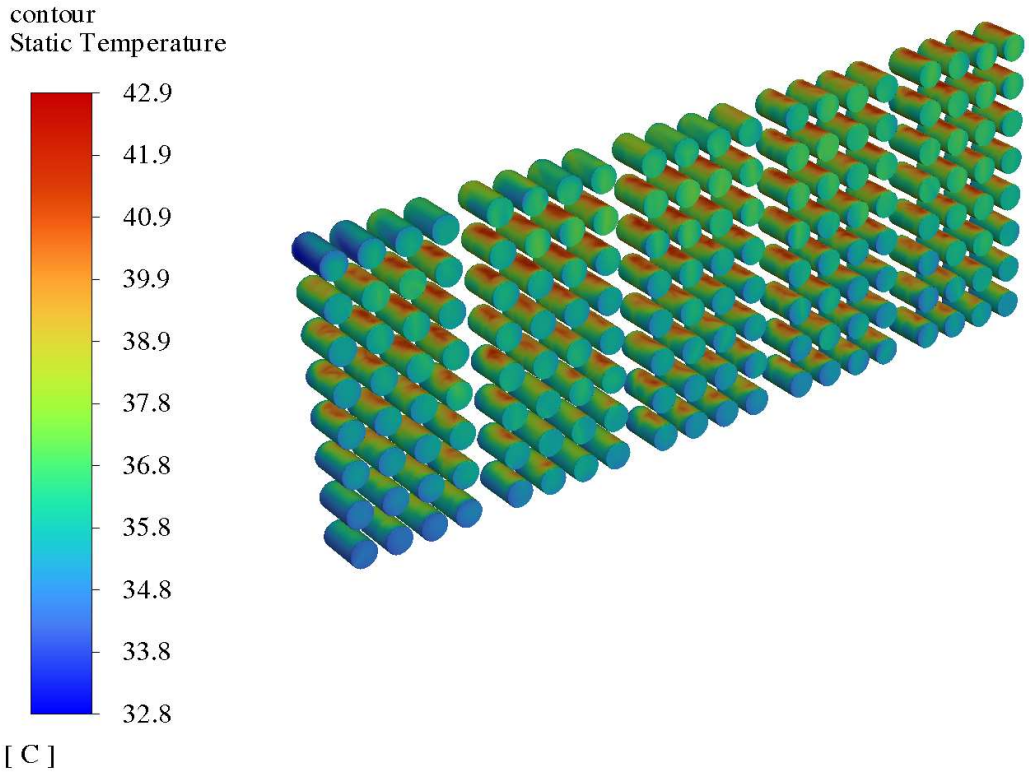

A2. Temperature Contour of Rack 2

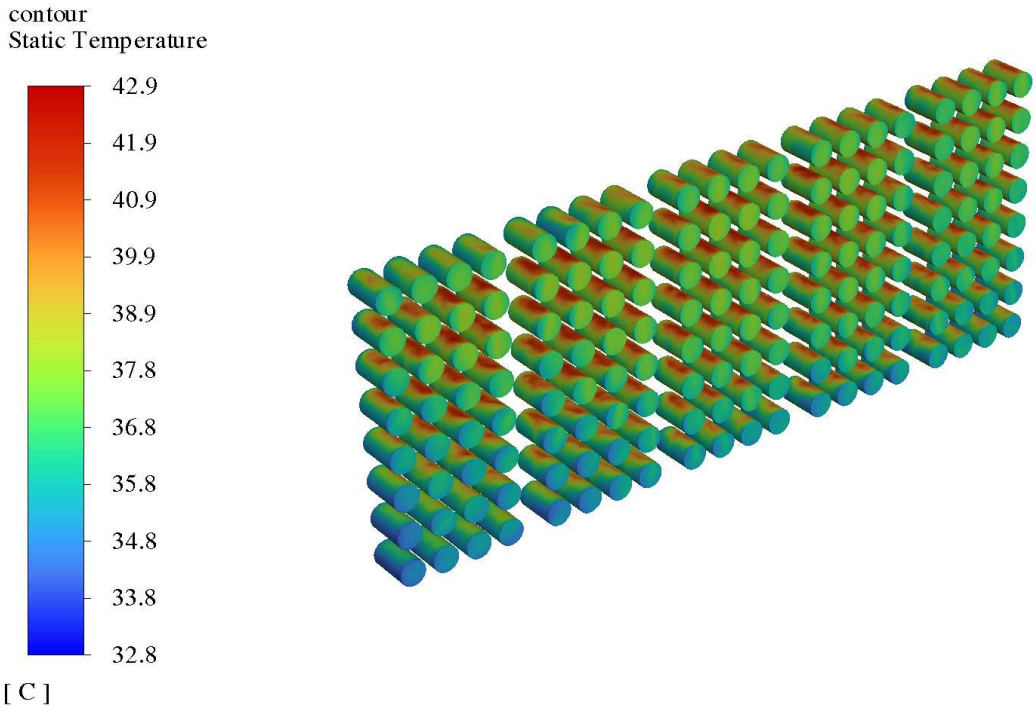

A3. Temperature Contour of Rack 3

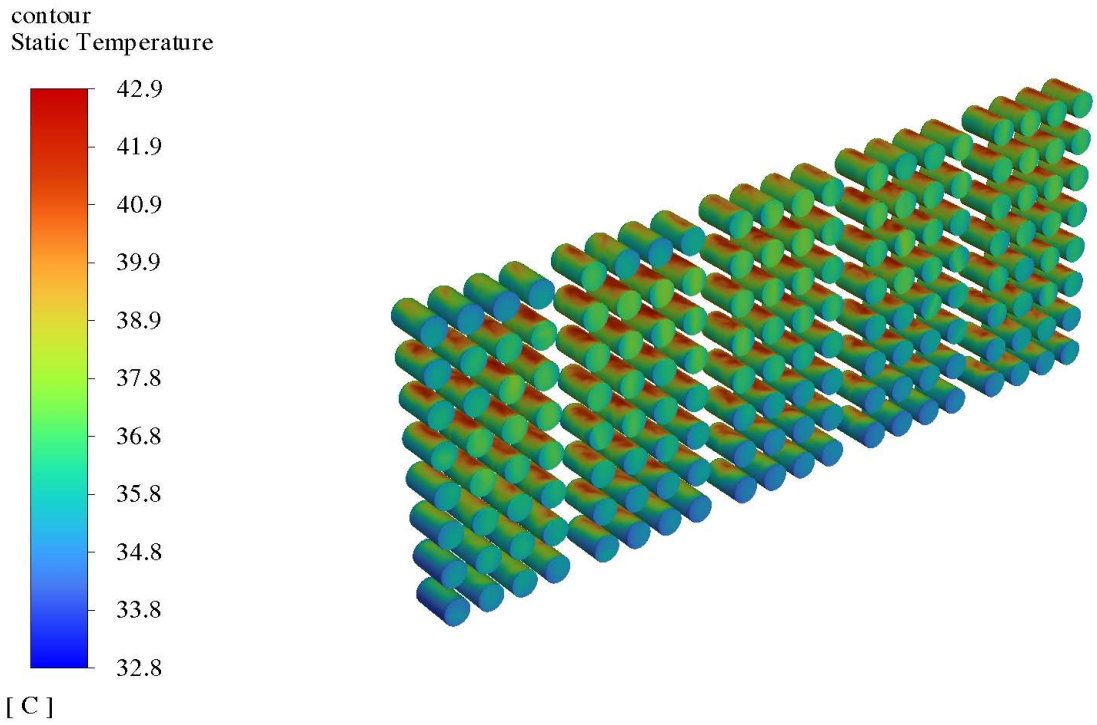

A4. Temperature Contour of Rack 4

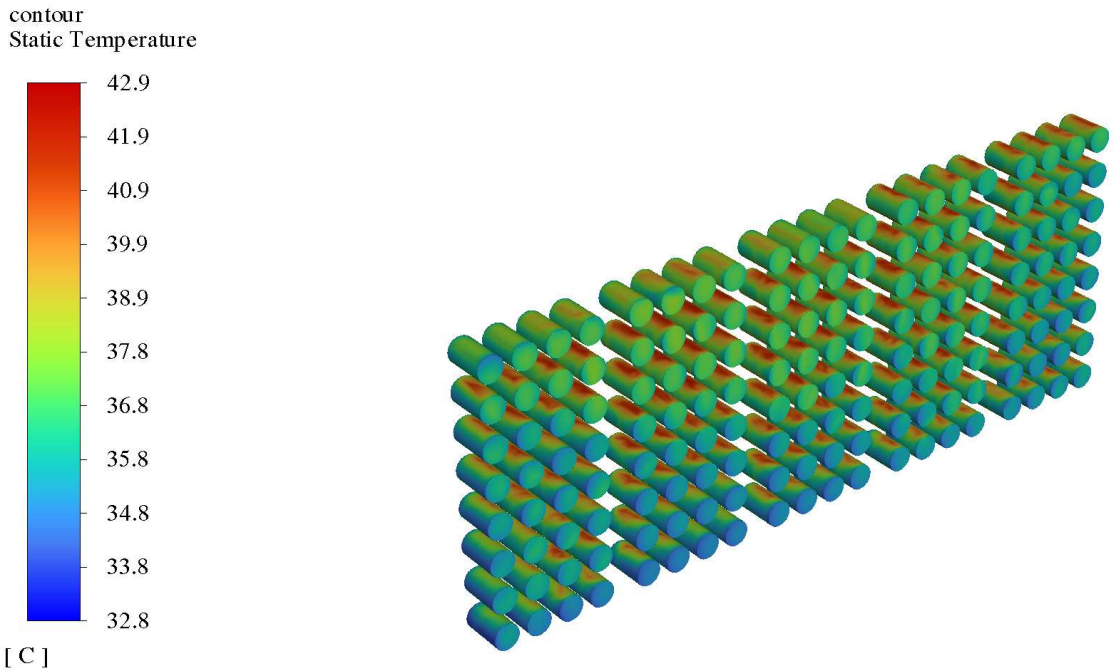

A5. Velocity Contours

X = 1.327 m Through Rack 1

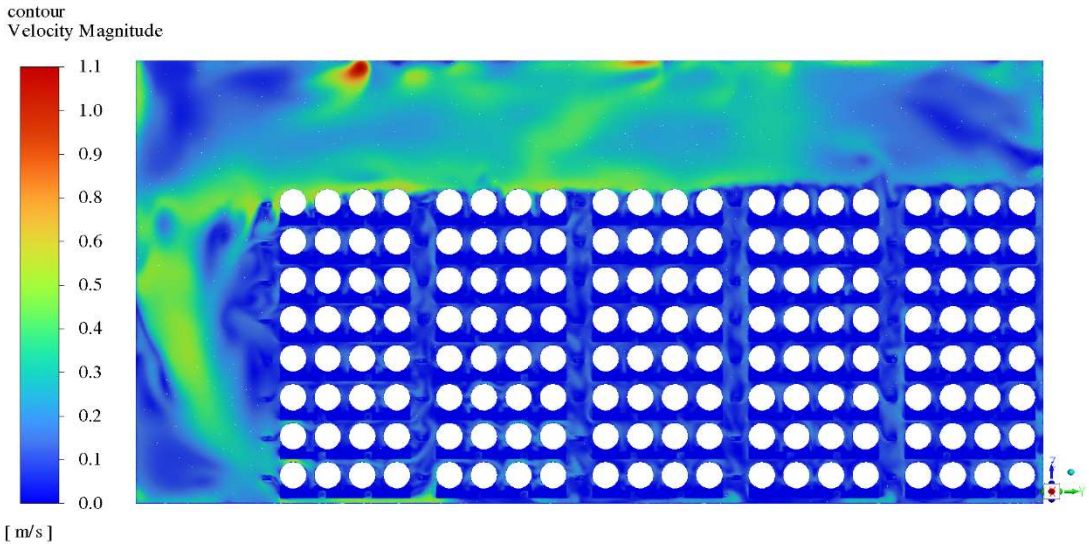

X = 1.688 m After Rack 1

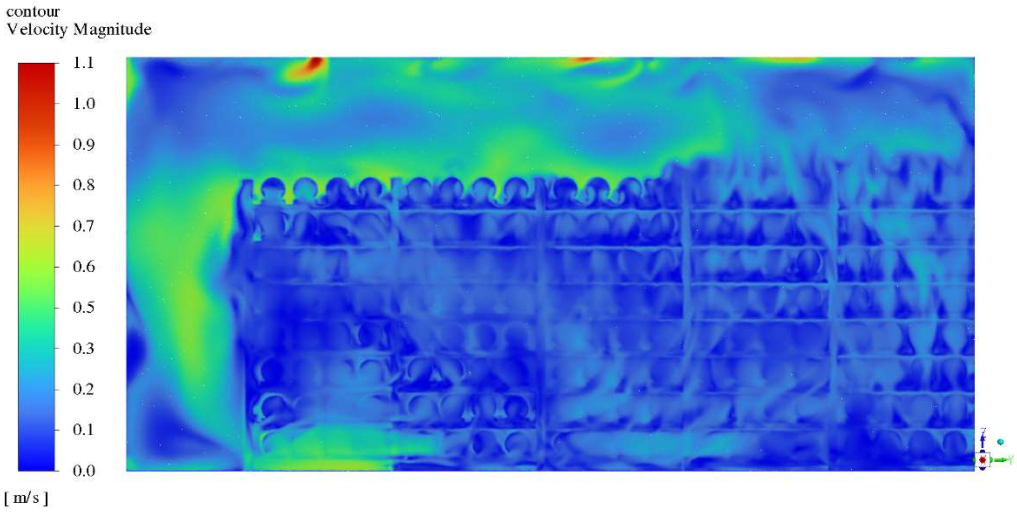

X = 2.2 m Between Rack 1 and 2

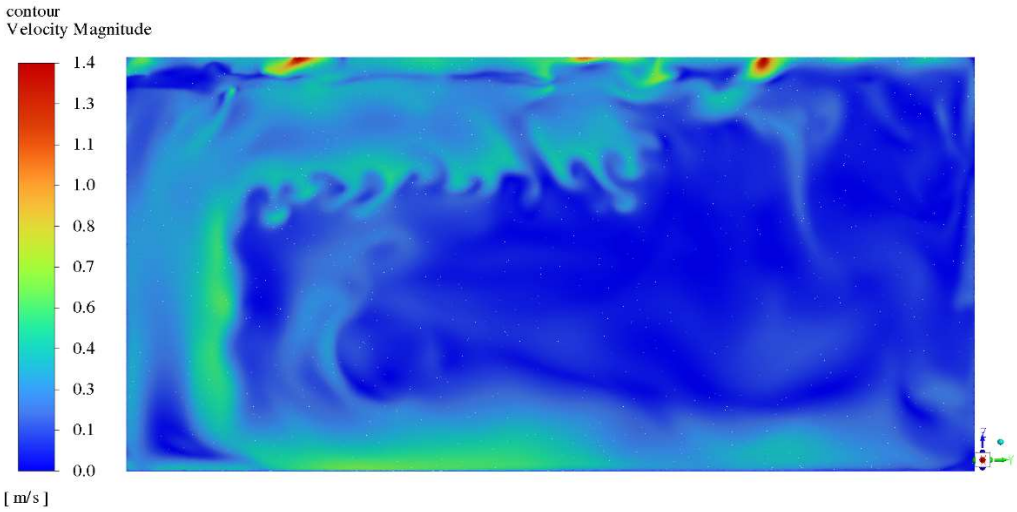

X = 3.518 m Before Rack 2

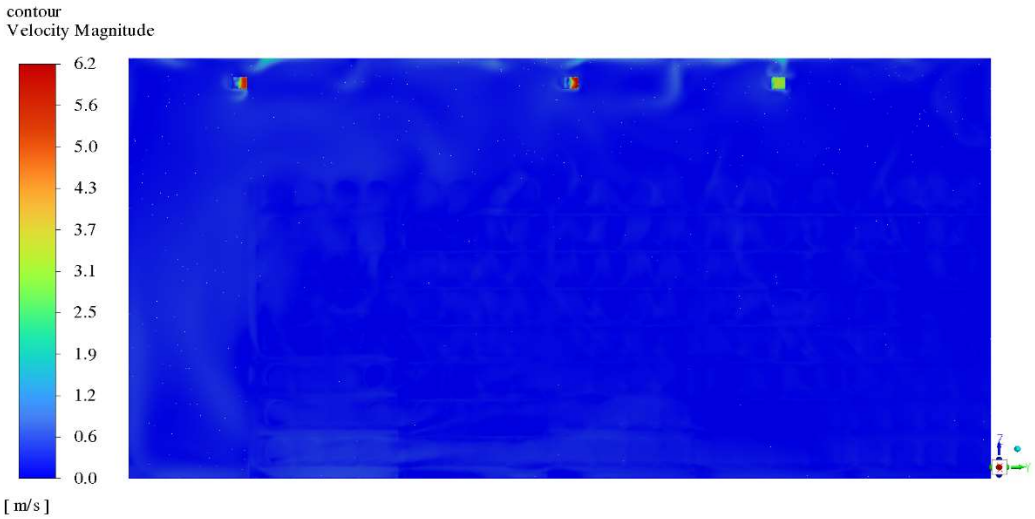

X = 3.989 m Through Rack 2

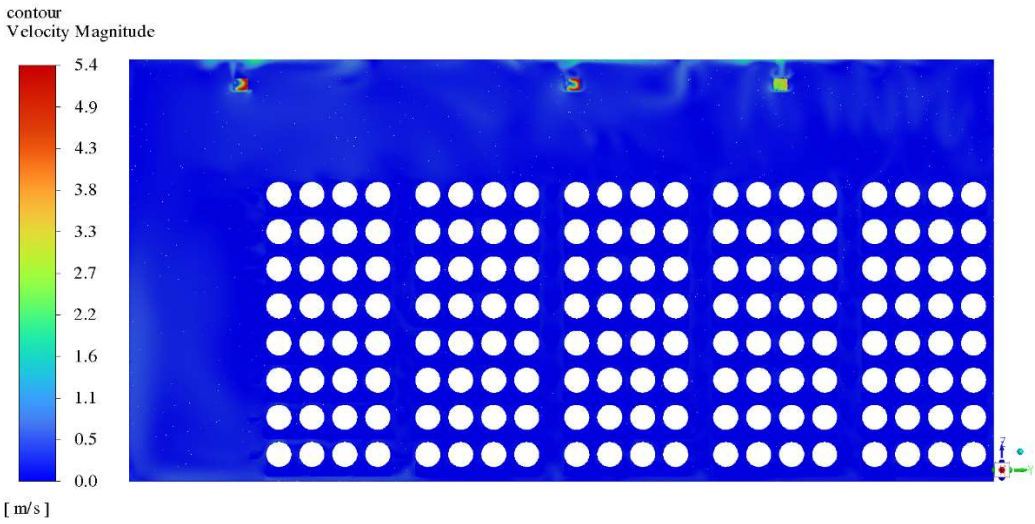

X = 4.572 m Between Rack 2 and 3

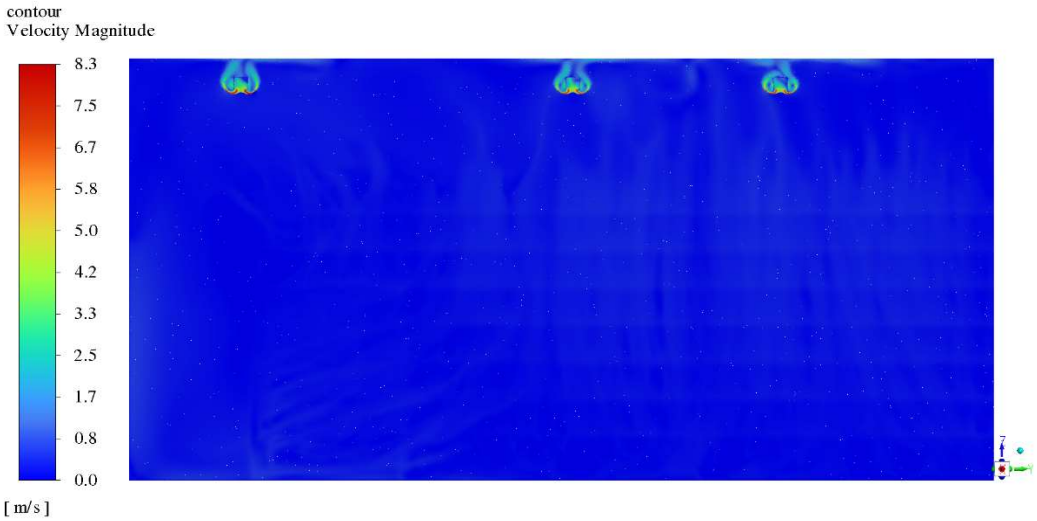

X = 5.043 m Through Rack 3

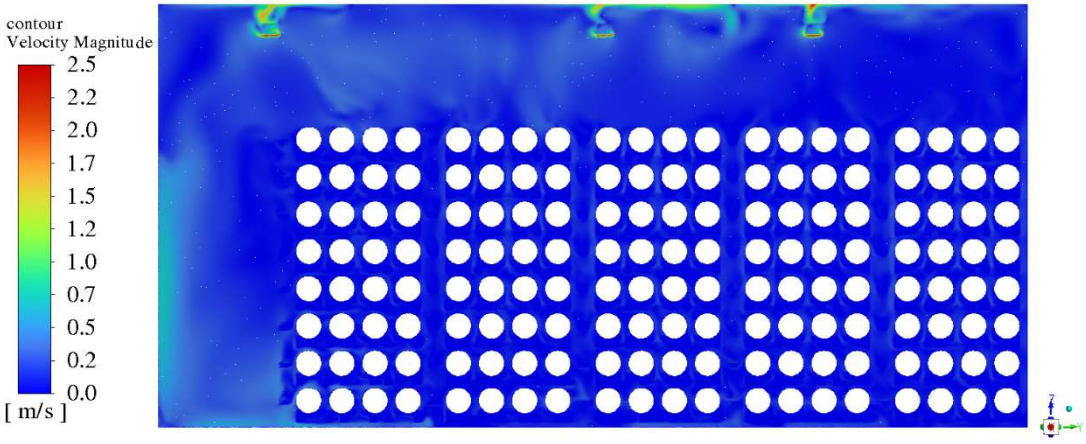

X = 5.612 m After Rack 3

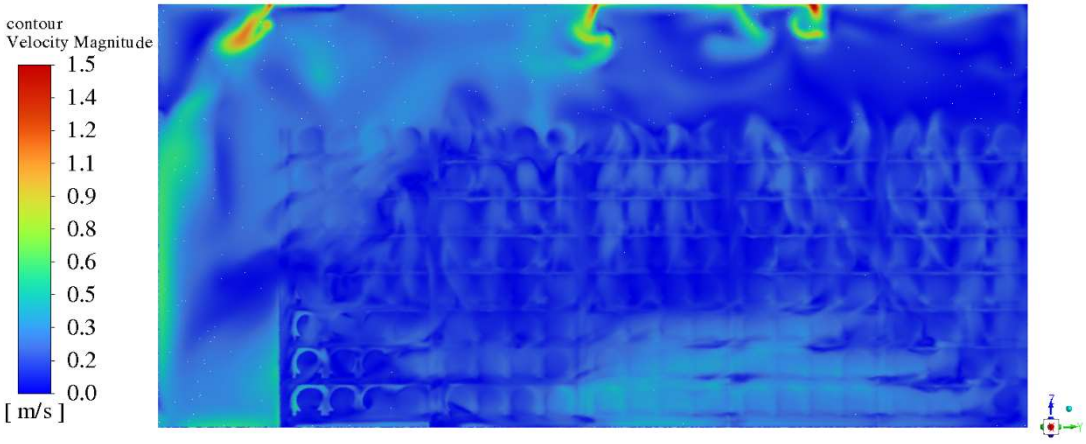

X = 6.472 m Between Rack 3 and 4

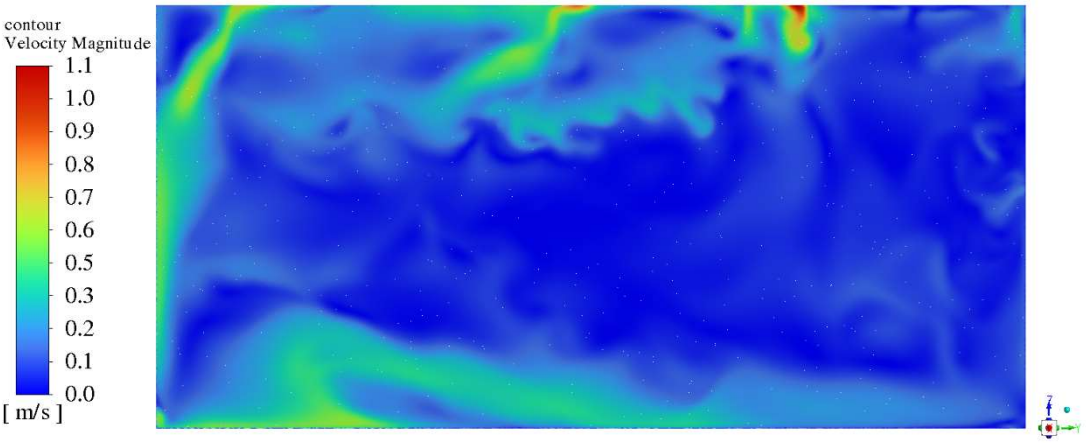

X = 7.4 m Before Rack 4

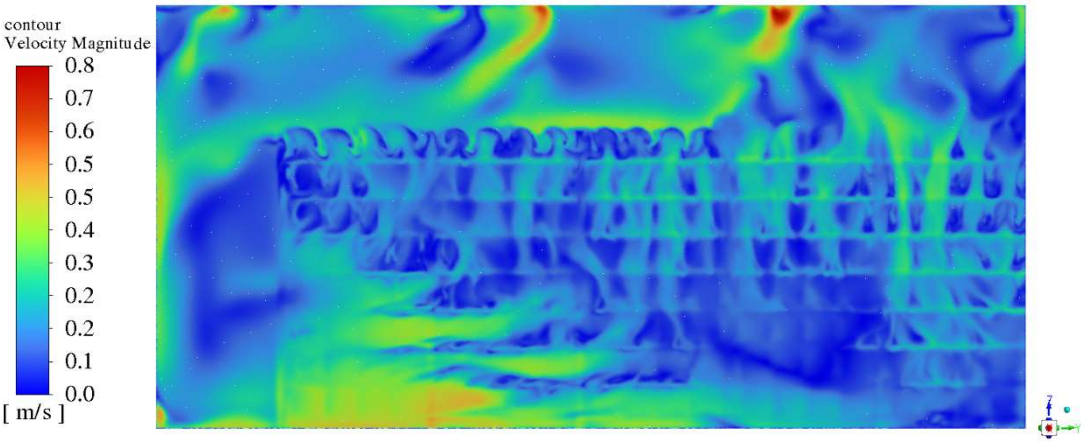

X = 7.87 m Through Rack 4

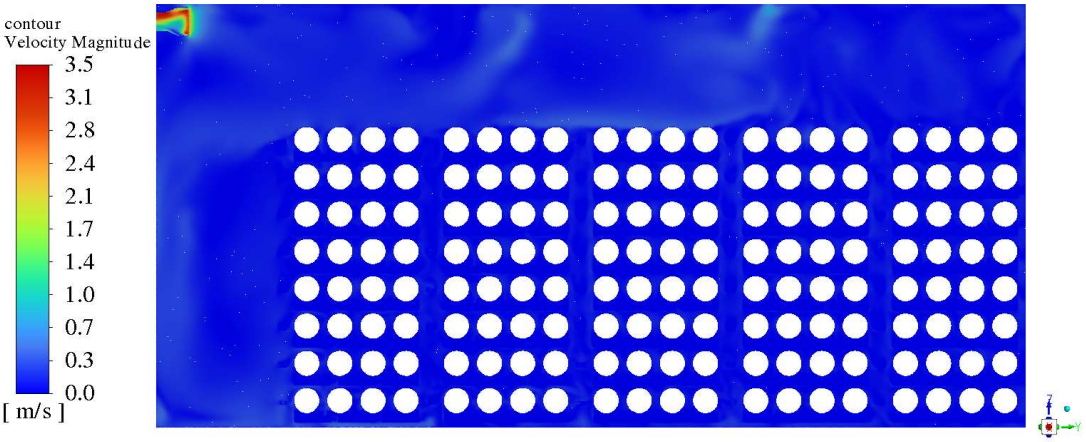

Y = 2.412 m Through Diffuser 1

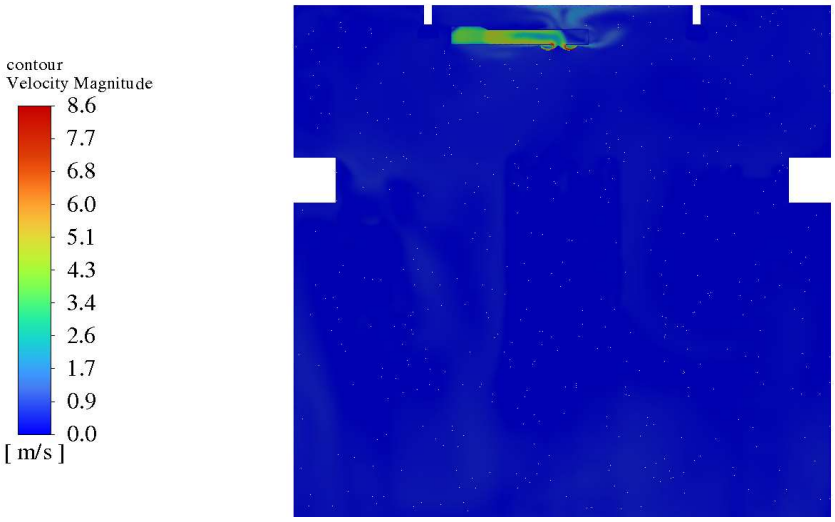

Y = 9.498 m Through Diffuser 2

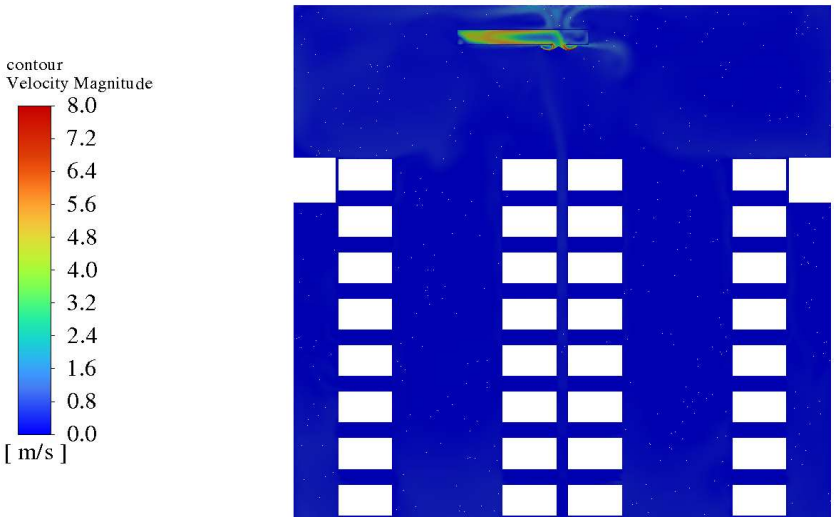

Y = 17.076 m Through Diffuser 3

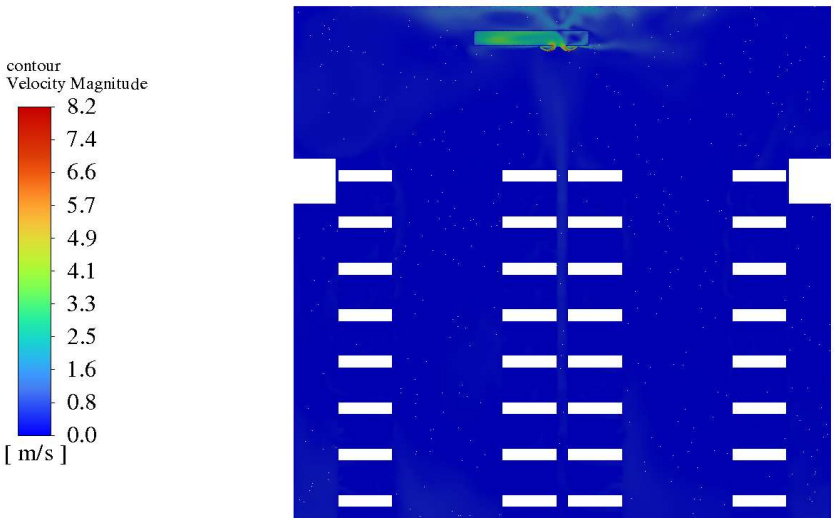

A6. Scaled Velocity Contours

X = 1.327 m Through Rack 1

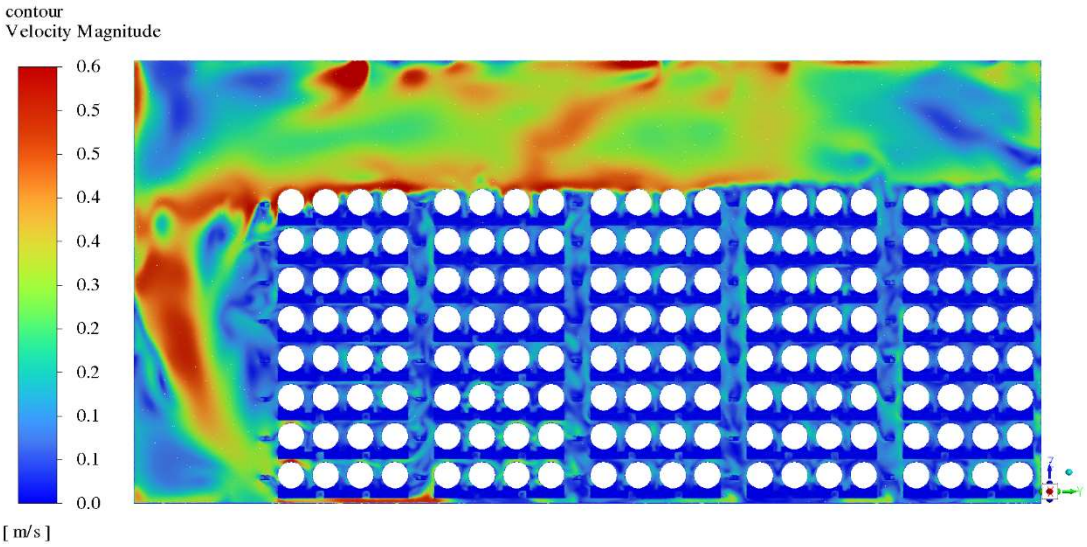

X = 1.688 m After Rack 1

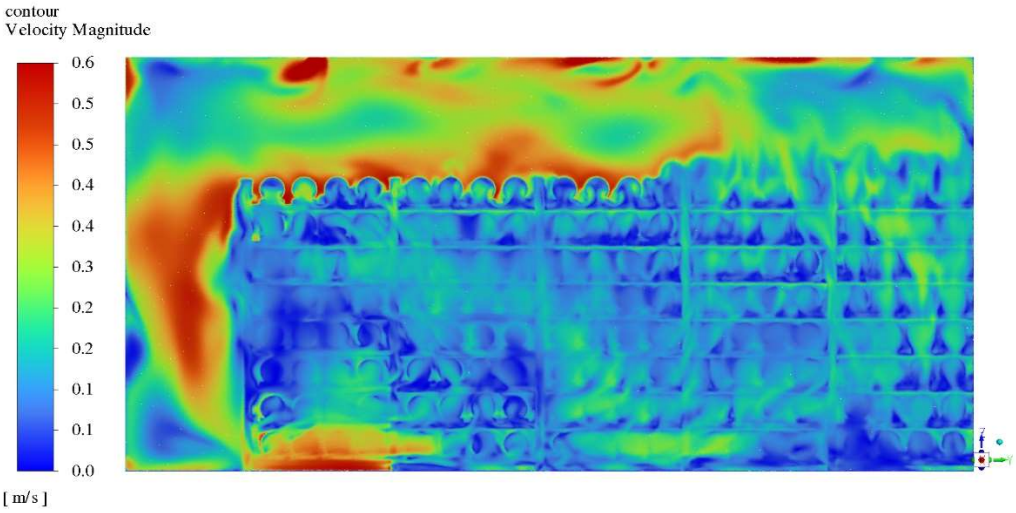

X = 2.2 m Between Rack 1 and 2

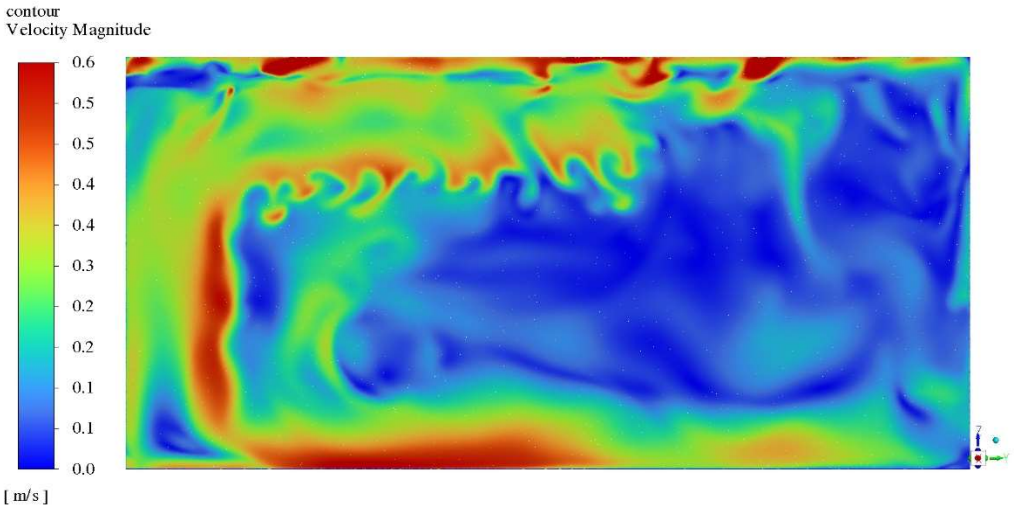

X = 3.518 m Before Rack 2

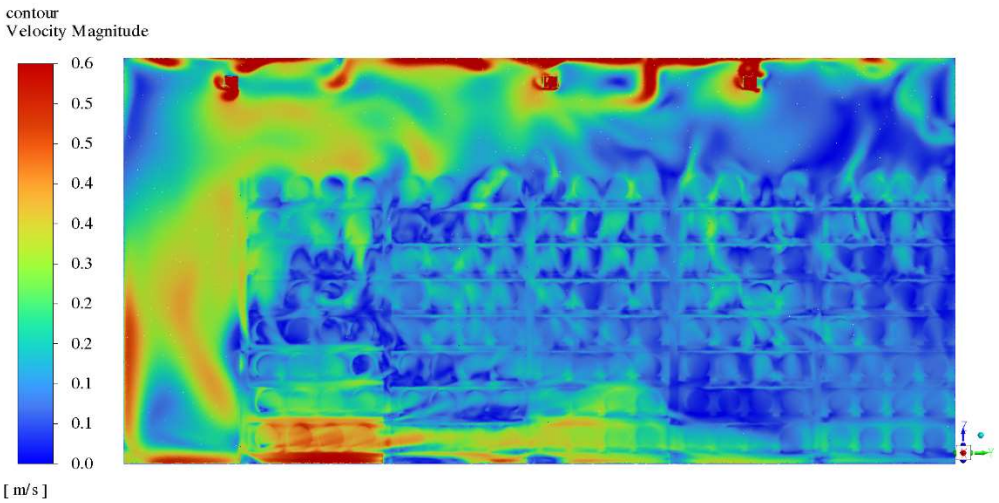

X = 3.989 m Through Rack 2

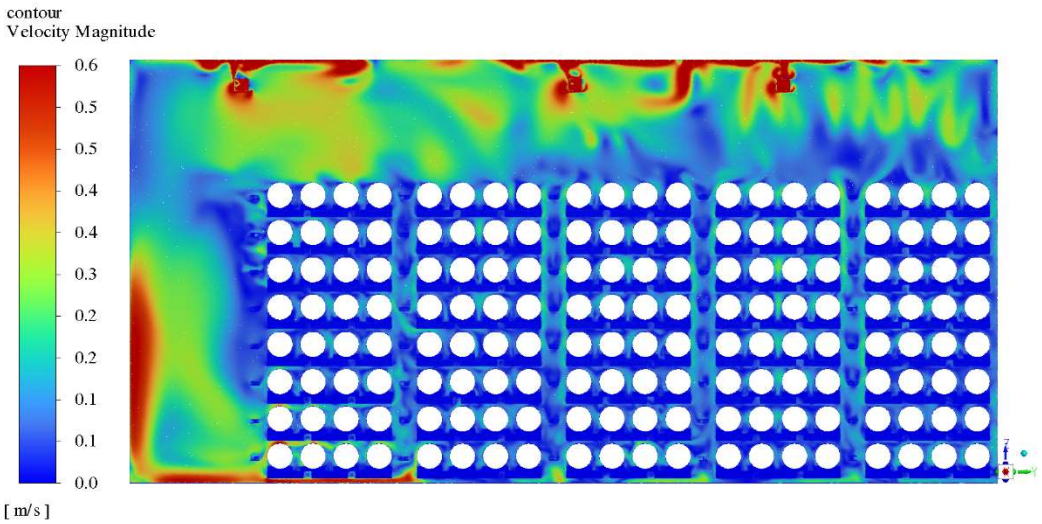

X = 4.572 m Between Rack 2 and 3

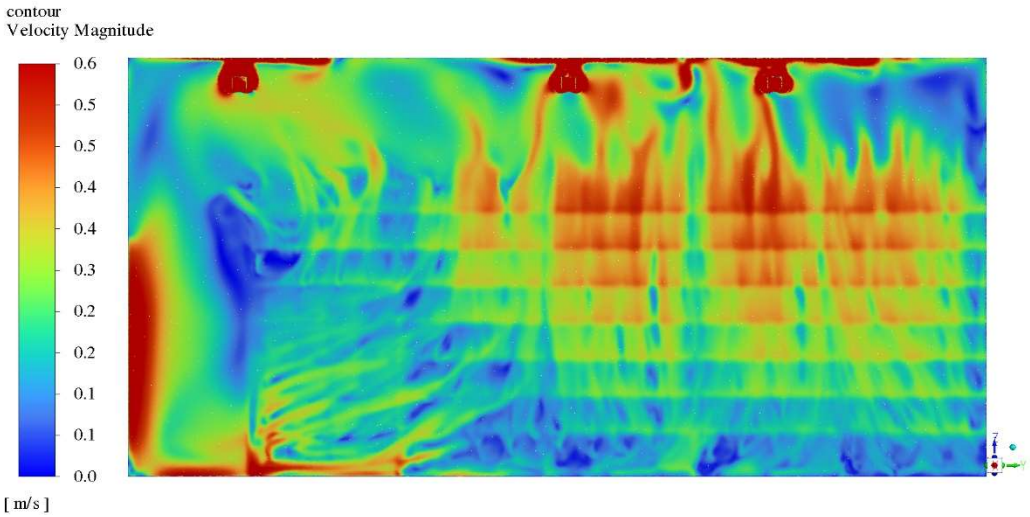

X = 5.043 m Through Rack 3

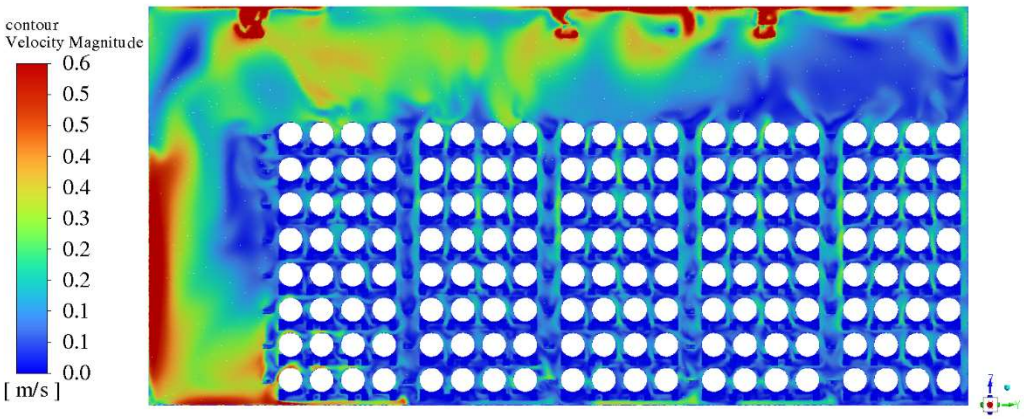

X = 5.612 m After Rack 3

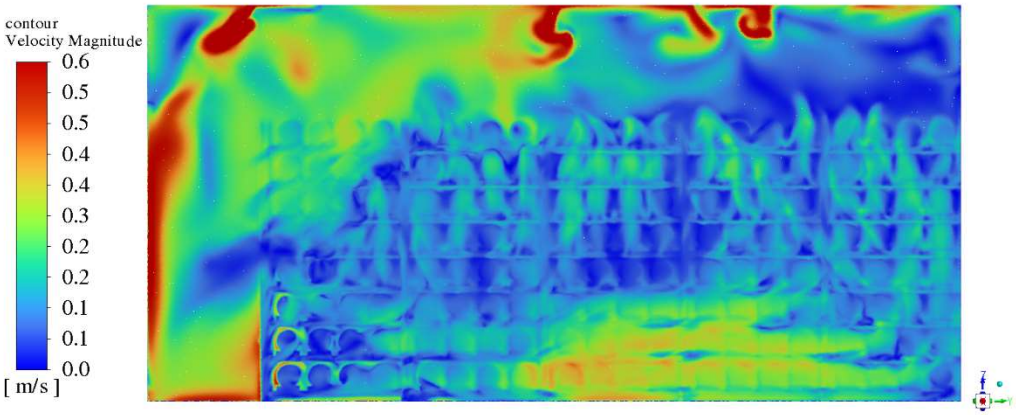

X = 6.472 m Between Rack 3 and 4

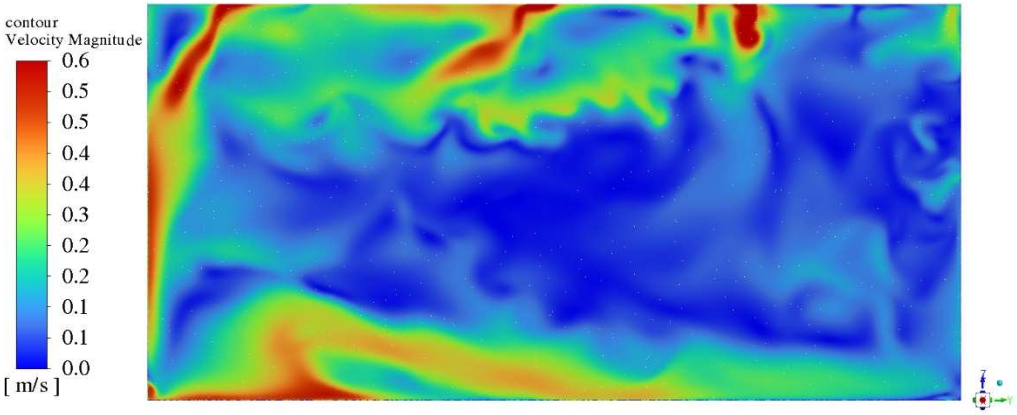

X = 7.4 m Before Rack 4

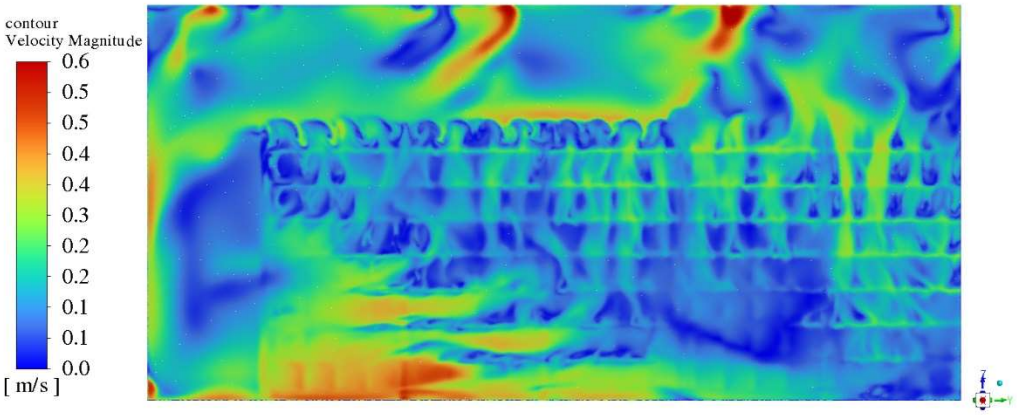

X = 7.87 m Through Rack 4

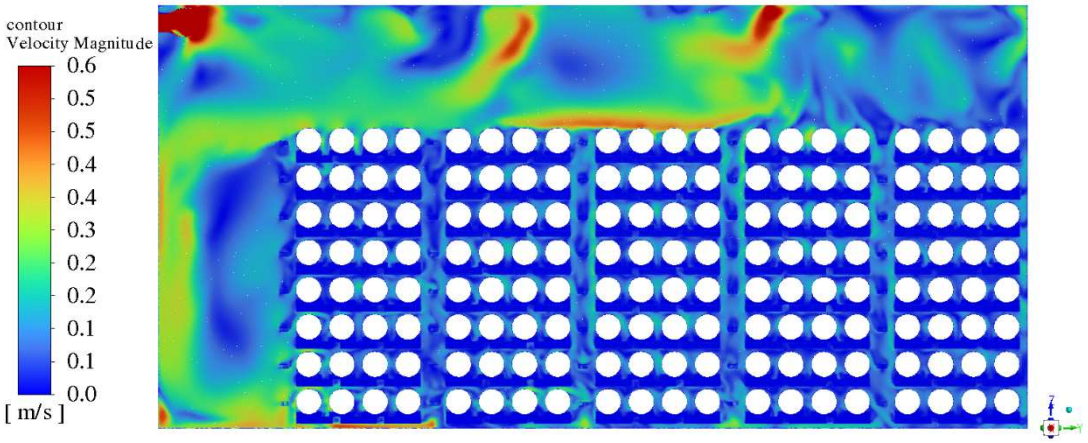

Y = 2.412 m Through Diffuser 1

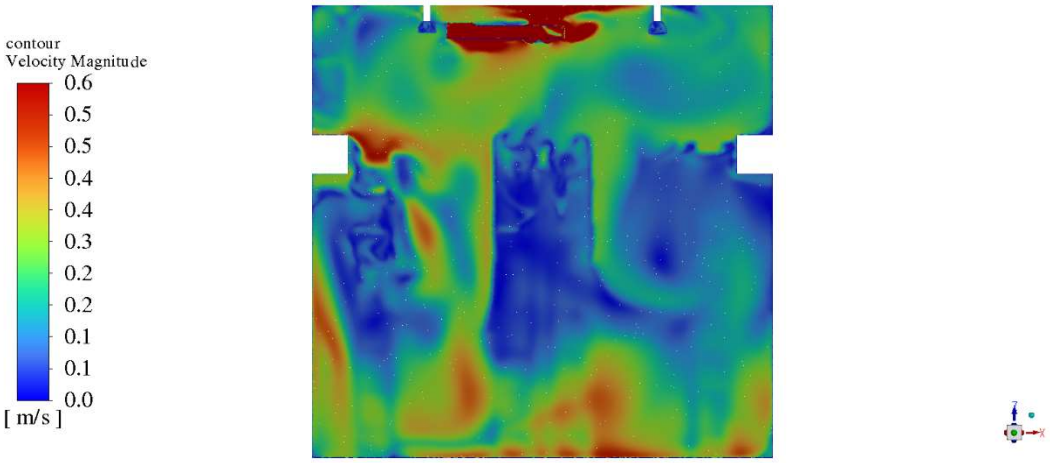

Y = 9.498 m Through Diffuser 2

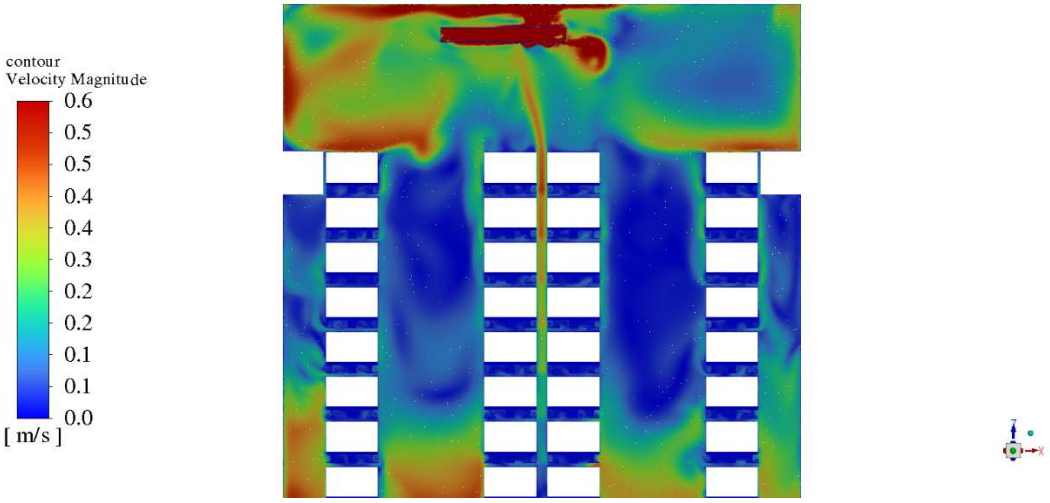

Y = 17.076 m Through Diffuser 3

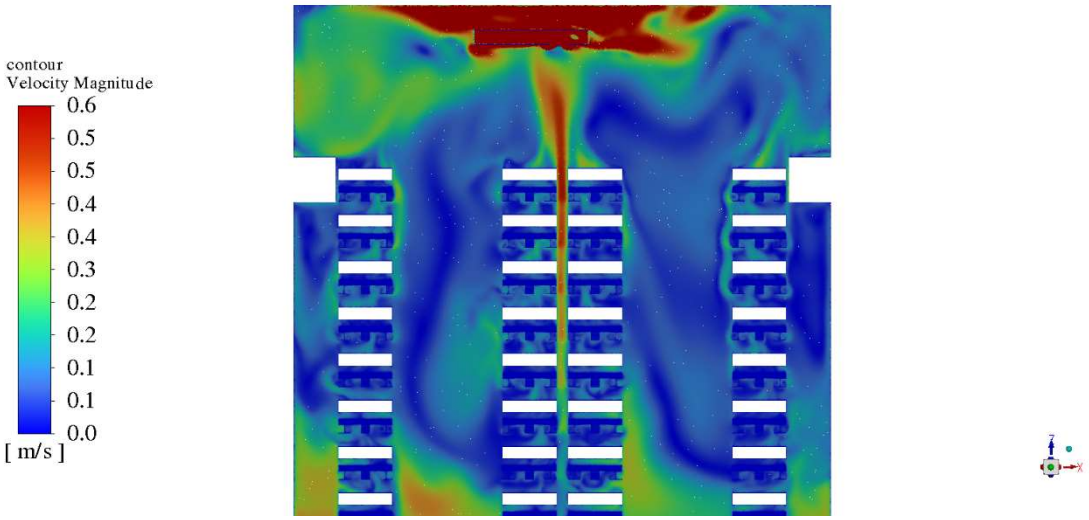

A7. Temperature Contours

X = 1.327 m Through Rack 1

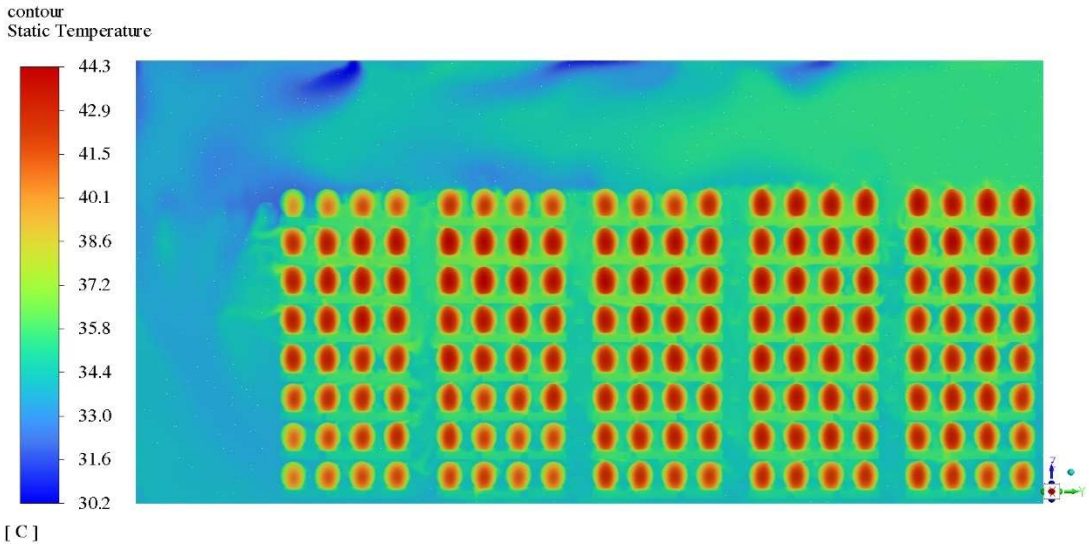

X = 1.688 m After Rack 1

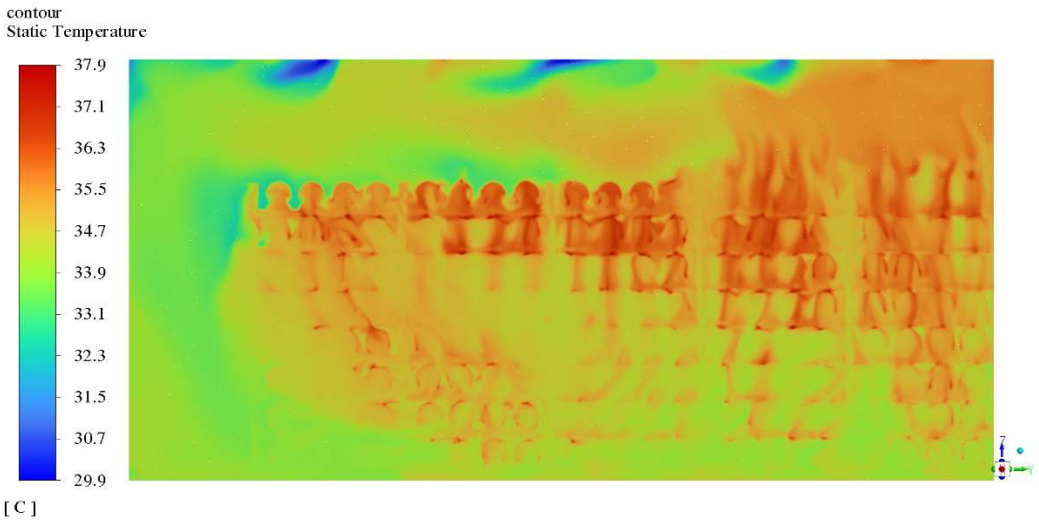

X = 2.2 m Between Rack 1 and 2

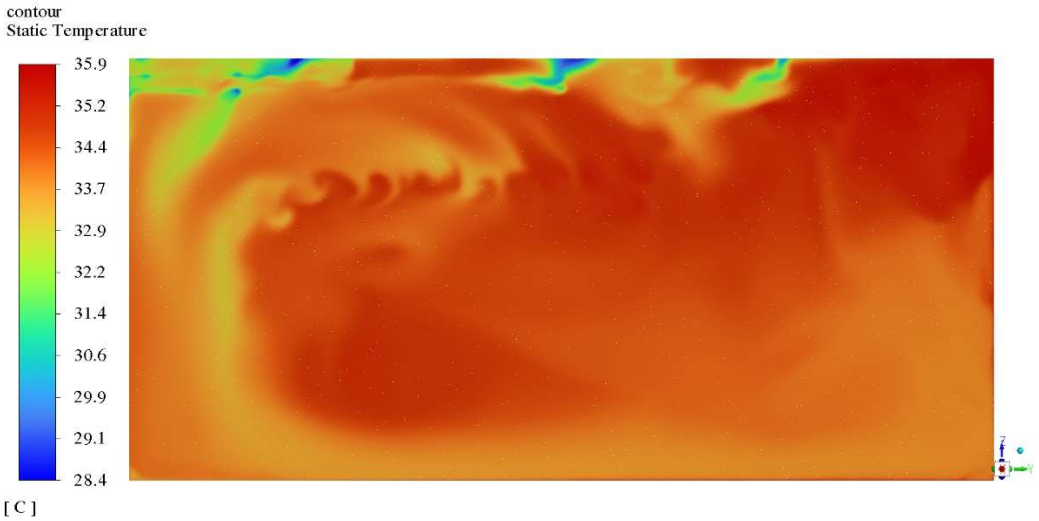

X = 3.518 m Before Rack 2

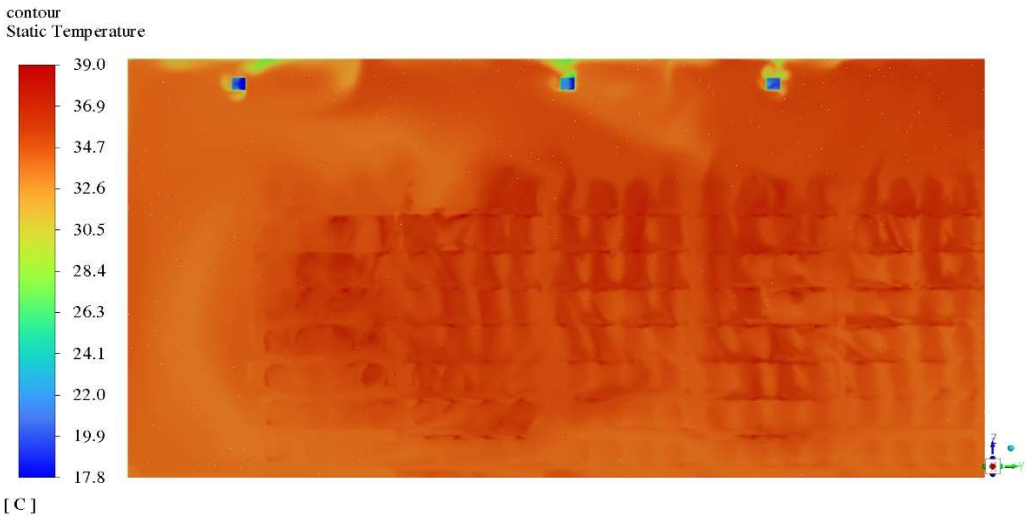

X = 3.989 m Through Rack 2

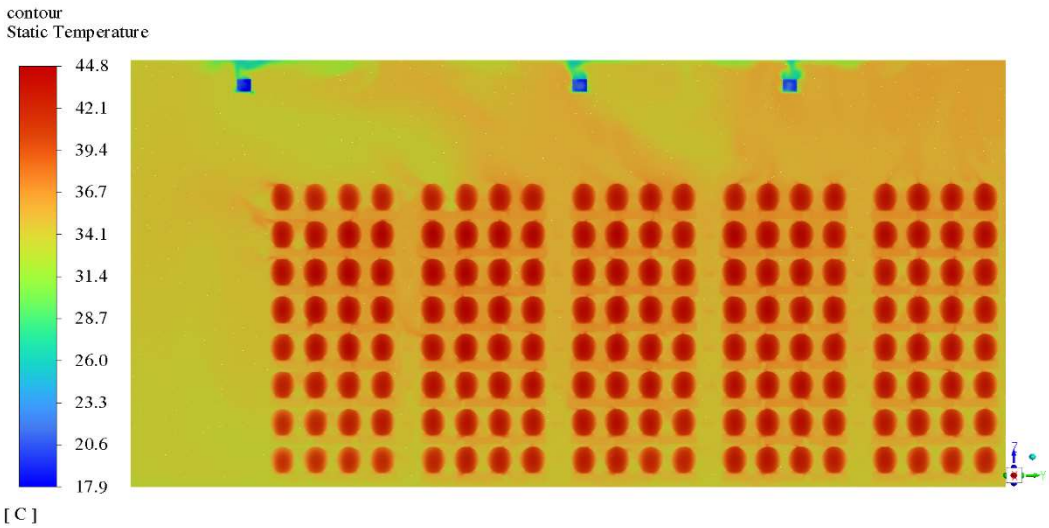

X = 4.572 m Between Rack 2 and 3

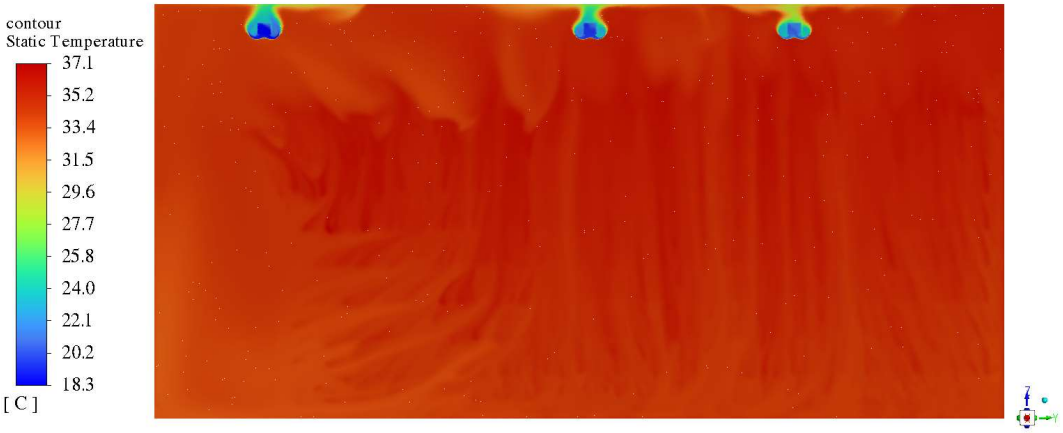

X = 5.043 m Through Rack 3

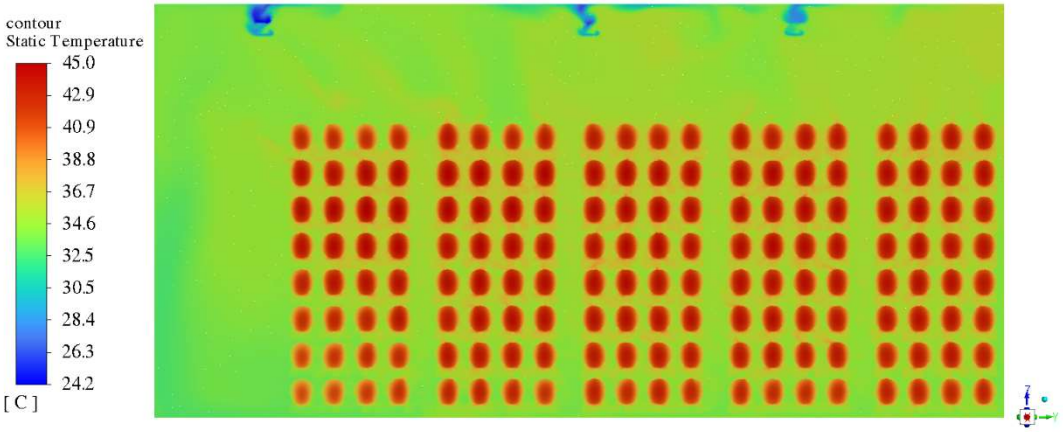

X = 5.612 m After Rack 3

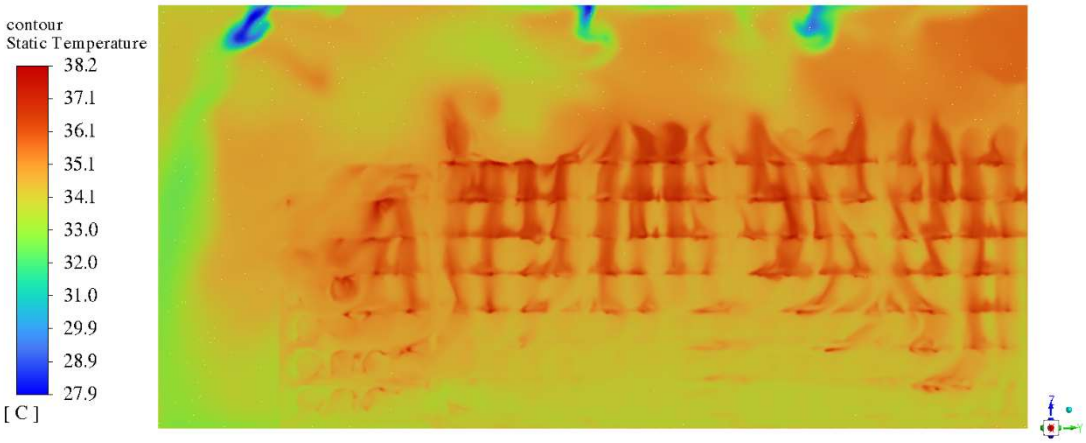

X = 6.472 m Between Rack 3 and 4

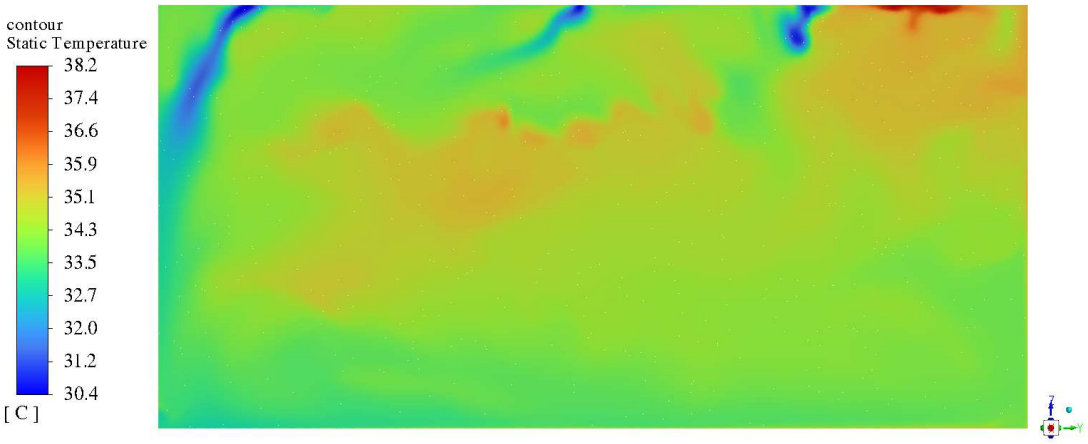

X = 7.4 m Before Rack 4

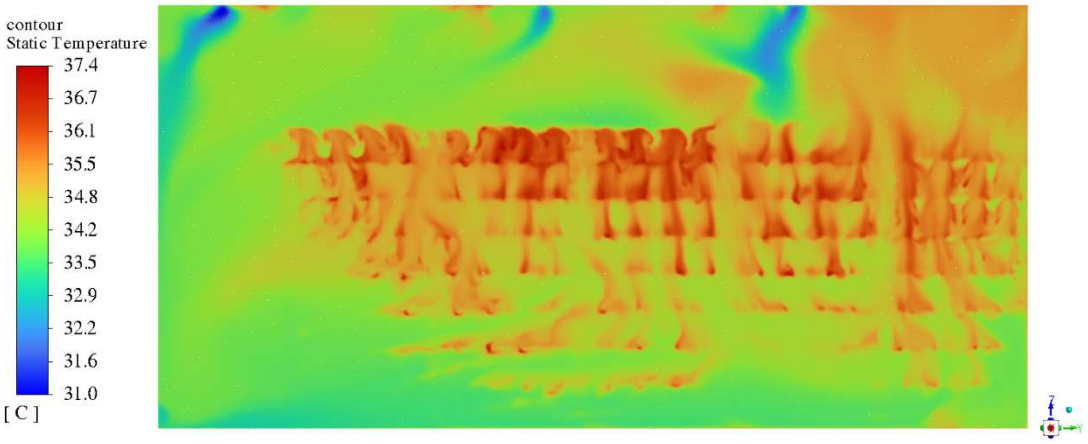

X = 7.87 m Through Rack 4

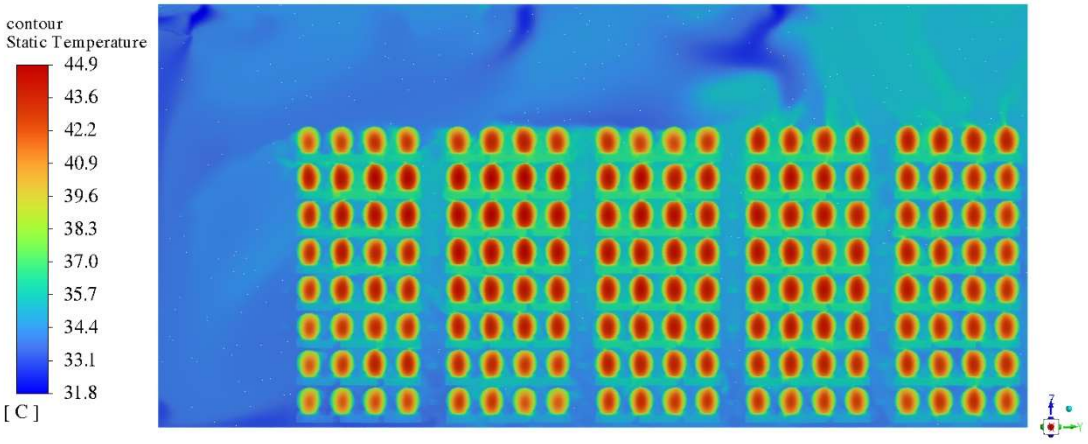

Y = 2.412 m Through Diffuser 1

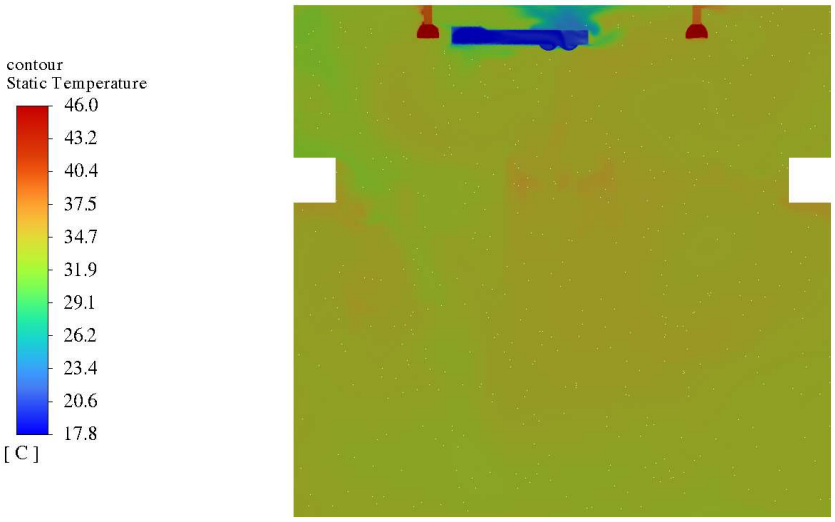

Y = 9.498 m Through Diffuser 2

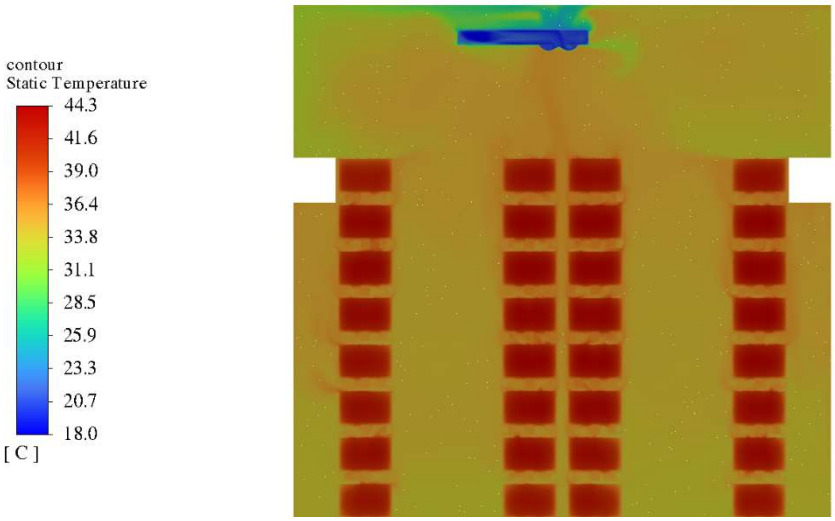

Y = 17.076 m Through Diffuser 3

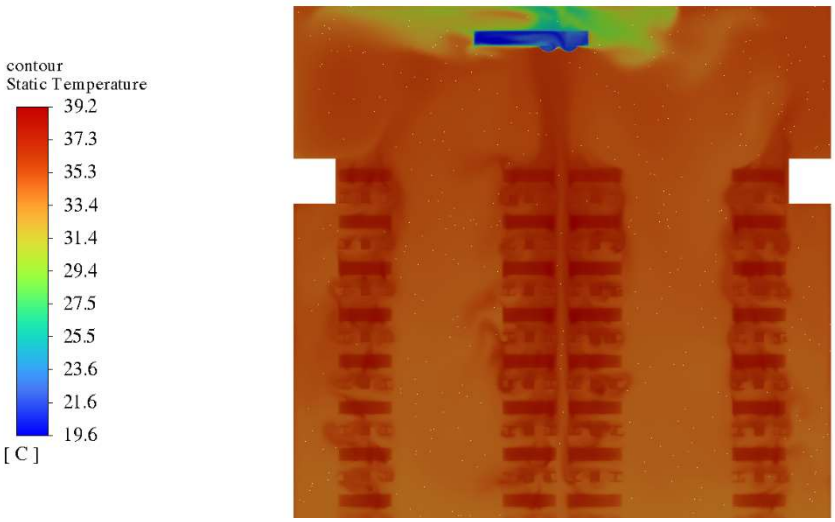

A8. Velocity Vectors

X = 1.327 m Through Rack 1

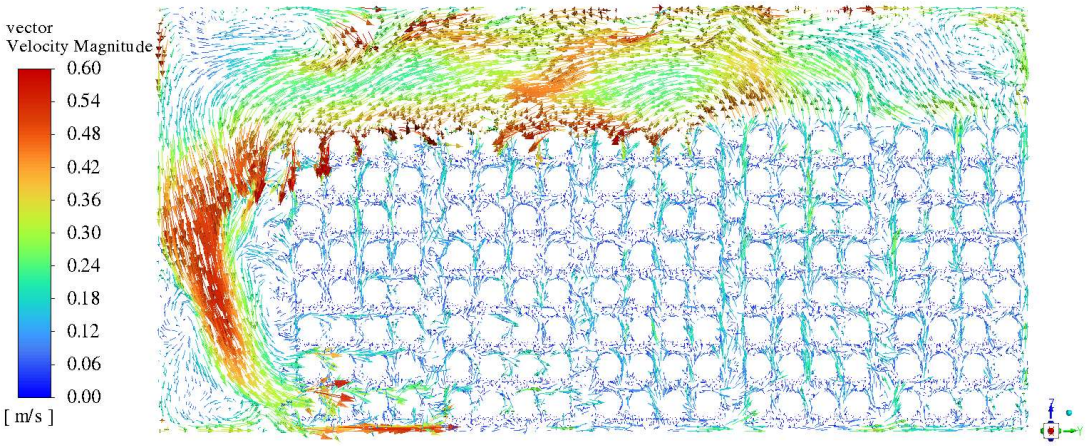

X = 2.2 m Between Rack 1 and 2

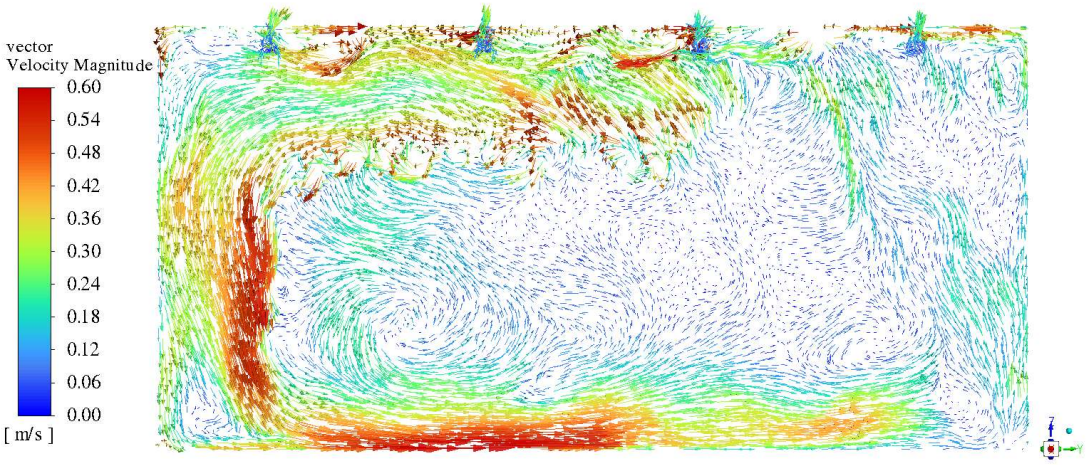

X = 3.518 m Before Rack 2

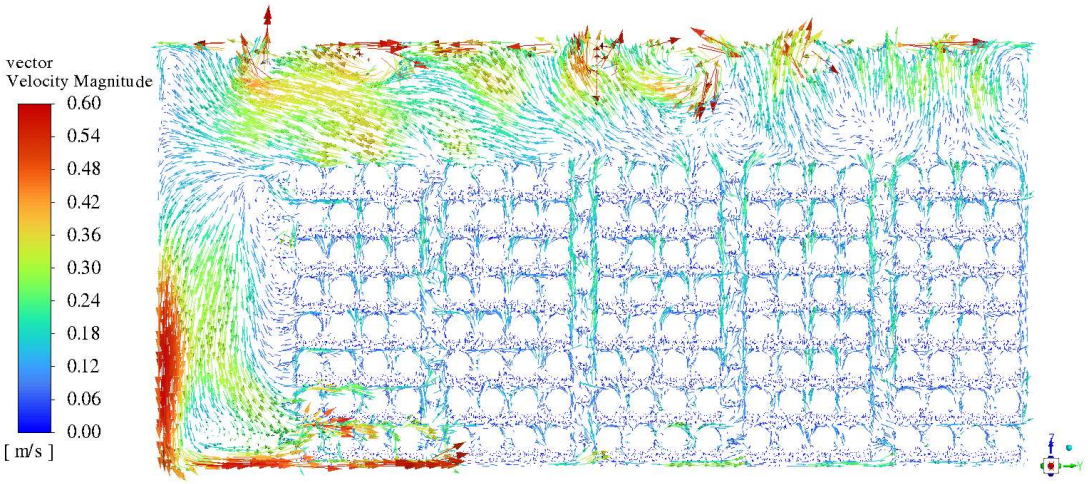

X = 3.989 m Through Rack 2

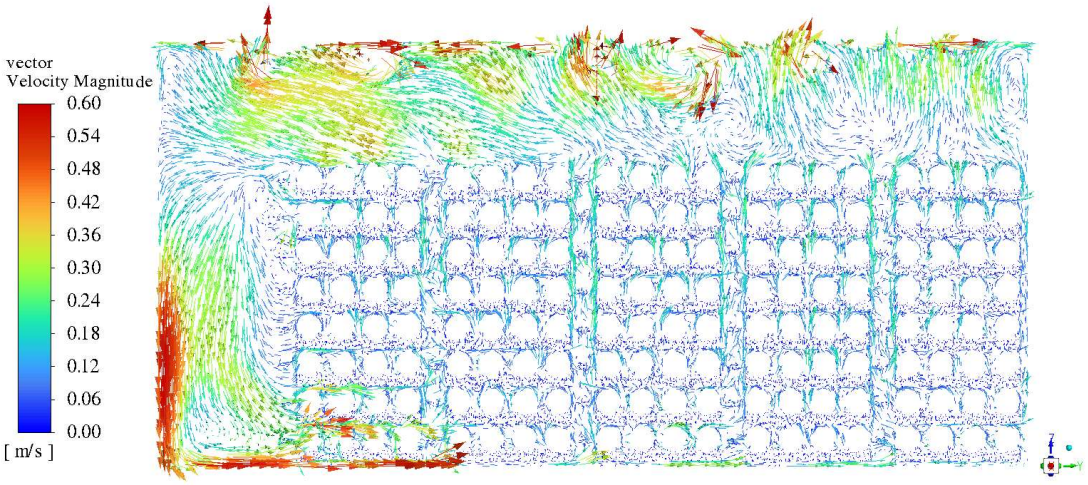

X = 4.572 m Between Rack 2 and 3

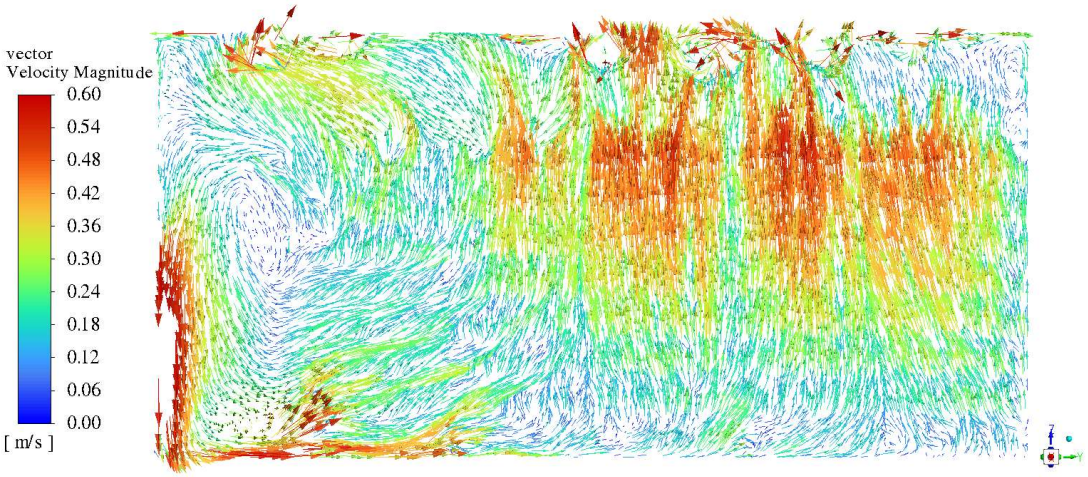

X = 5.043 m Through Rack 3

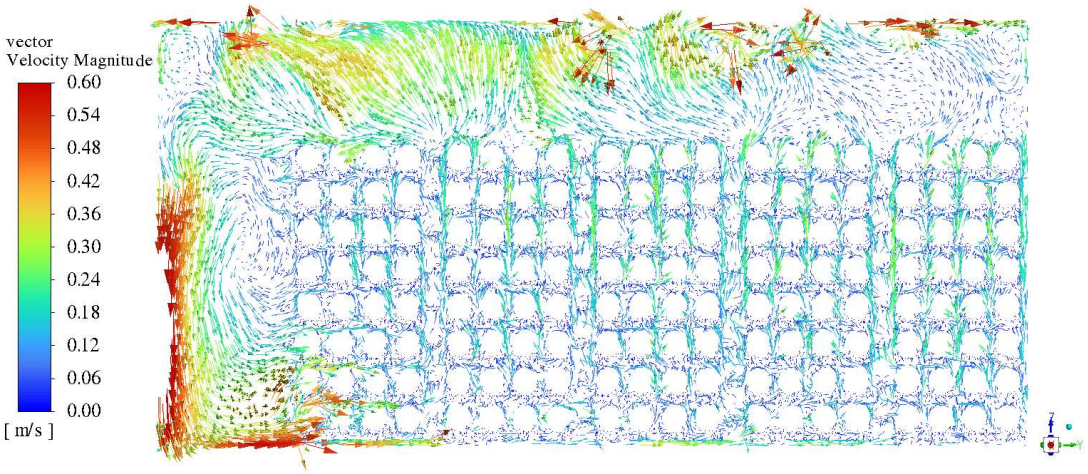

X = 5.612 m After Rack 3

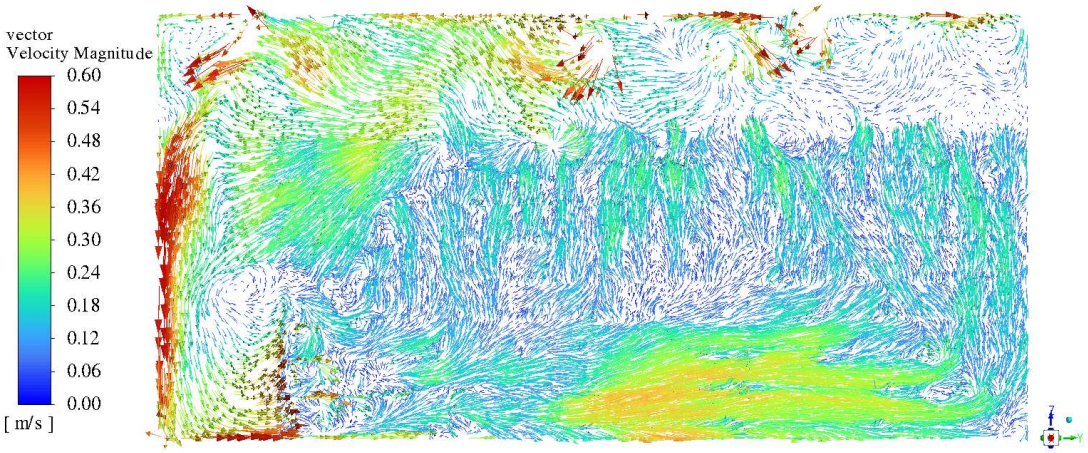

X = 6.472 m Between Rack 3 and 4

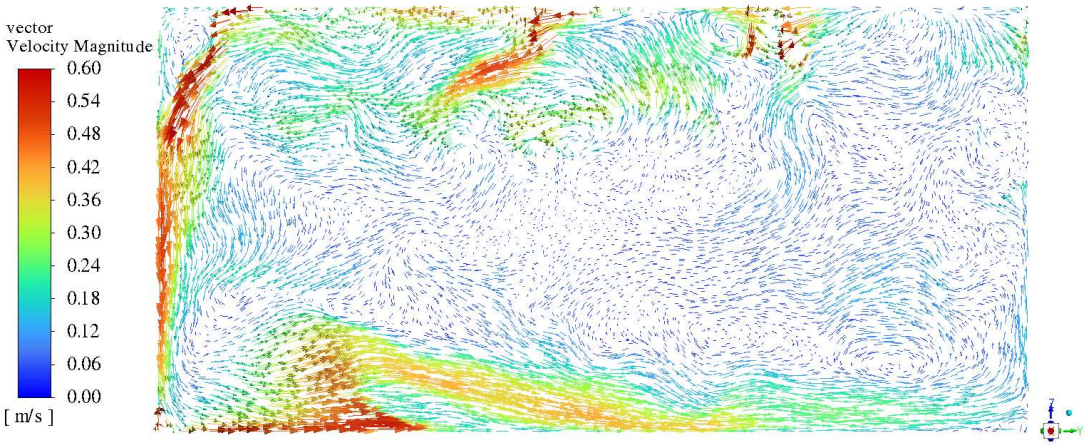

X = 7.4 m Before Rack 4

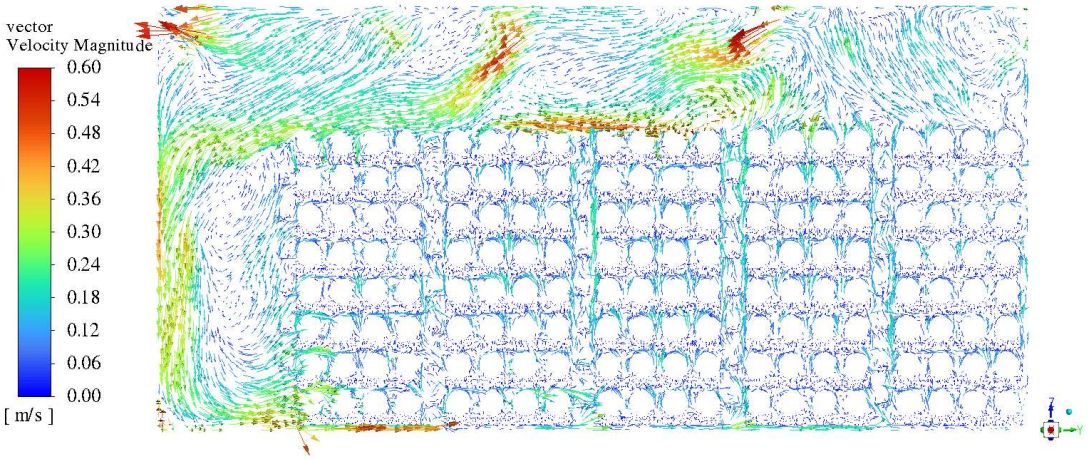

X = 7.87 m Through Rack 4

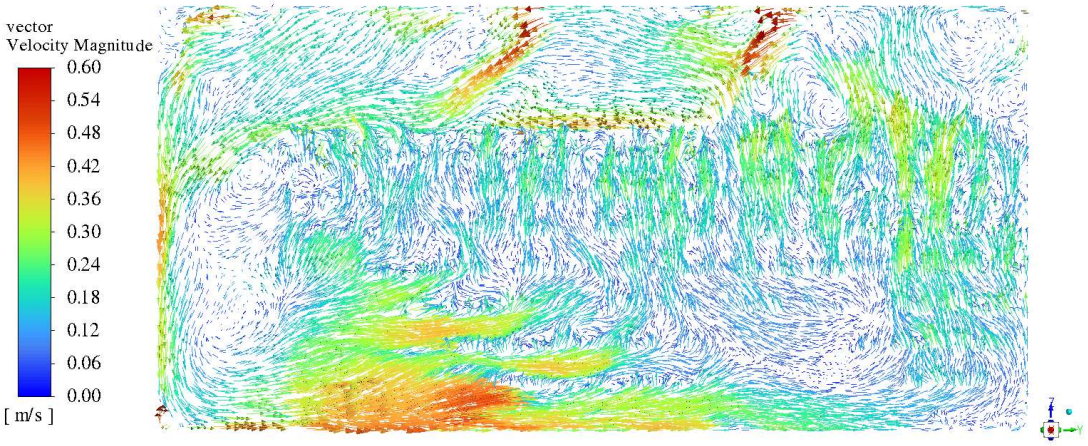

Y = 2.412 m Through Diffuser 1

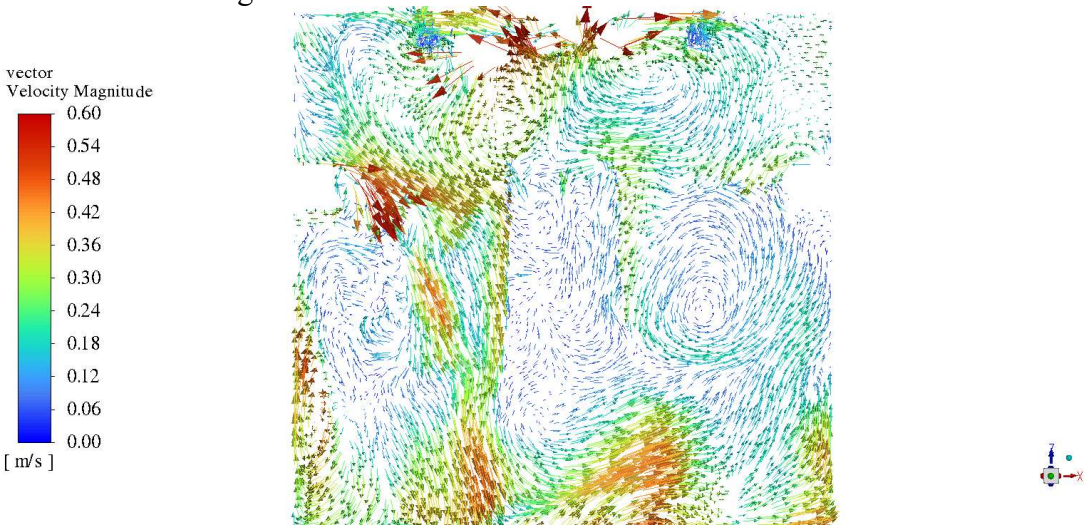

Y = 9.498 m Through Diffuser 2

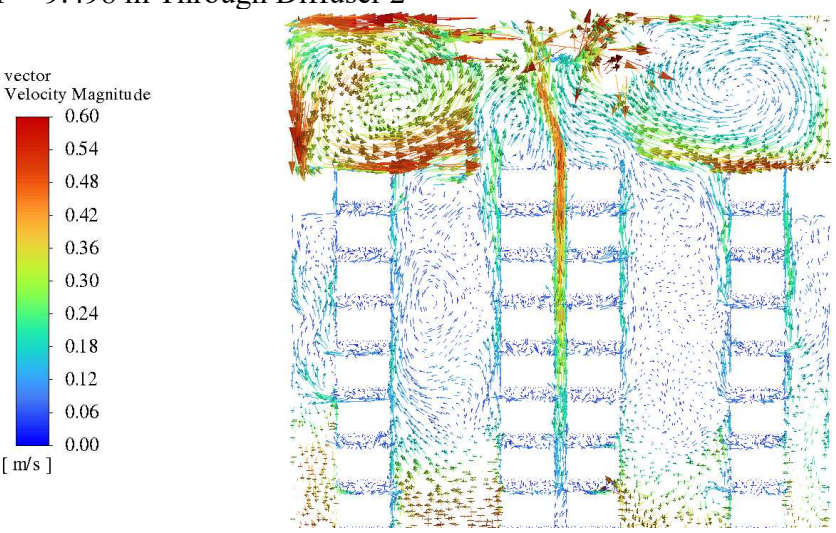

Y = 17.076 m Through Diffuser 3